Supplemental Information

Phosphoproteomic quantitation and causal analysis reveal pathways in GPVI/ITAM-mediated platelet activation programs

Özgün Babur, Alexander R. Melrose, Jennifer M. Cunliffe, John Klimek, Jiaqing Pang, Anna-Liisa I. Sepp, Jevgenia Zilberman-Rudenko, Samuel Tassi Yunga, Tony Zheng, Iván Parra-Izquierdo, Jessica Minnier, Owen J. T. McCarty, Emek Demir, Ashok P. Reddy, Phillip A. Wilmarth, Larry L. David, and Joseph E. Aslan

Supplemental Data Availability

Mass Spectrometry Data Files – Mass spectrometry (MS) data – including MS data files and Jupyter notebook files detailing data analyses – have been deposited to the ProteomeXchange Consortium via the PRIDE partner repository[1] with the dataset identifier PXD017167.

Interactive Data Analysis Tools

• Interactive and searchable results of phosphoproteomics data analysis and graphs are hosted by "The START app" through Shiny at:

Condition #1; pTyr enrichment: https://kcvi.shinyapps.io/STARTapp_359-pTyr/

Condition #1; TiO2 enrichment: https://kcvi.shinyapps.io/STARTapp_359_TiO2/

Condition #2; pTyr enrichment: https://kcvi.shinyapps.io/STARTapp_515_pTyr/

Condition #2; TiO2 enrichment: https://kcvi.shinyapps.io/STARTapp_515_TiO2/

• Pathway maps related to Figures 4B and S8-13 are available via Newt Pathway Viewer & Editor[2] at:

Summary Model (Figure 4B):
http://web.newteditor.org/?URL=https://raw.githubusercontent.com/PathwayAndDataAnalysis/repo/master/newt-files/Blood-2020/Fig4B.nwt

Causal (and unmapped) Relations for Condition #1 (Figure S8, S12):
http://web.newteditor.org/?URL=https://raw.githubusercontent.com/PathwayAndDataAnalysis/repo/master/newt-files/Blood-2020/Cond1Causative.nwt

Causal (and unmapped) Relations for Condition #2 (Figure S9, S13):
http://web.newteditor.org/?URL=https://raw.githubusercontent.com/PathwayAndDataAnalysis/repo/master/newt-files/Blood-2020/Cond2Causative.nwt

Conflicting Relations for Condition #1 (Figure S10):
http://web.newteditor.org/?URL=https://raw.githubusercontent.com/PathwayAndDataAnalysis/repo/master/newt-files/Blood-2020/Cond1Conflicting.nwt

Conflicting Relations for Condition #2 (Figure S11):
http://web.newteditor.org/?URL=https://raw.githubusercontent.com/PathwayAndDataAnalysis/repo/master/newt-files/Blood-2020/Cond2Conflicting.nwt

Supplemental Materials and Methods

All reagents were from Sigma-Aldrich (St. Louis, MO, USA), unless otherwise noted. PGI_2 was from Cayman Chemical (Ann Arbor, MI, USA). Crosslinked collagen-related peptide (CRP-XL, or, CRP) was from R. Farndale (CambCol Laboratories, Cambridge University, UK). ACT017 was from Martine Jandrot-Perrus (INSERM, France). Chrono-lume detection agent was from Chrono-Log Corporation (Havertown, PA, USA). Fibrinogen (FIB3) was from Enzyme Research. U46619 was from Tocris. Phos-tag acrylamide was from ApexBio. TXB2 ELISA kit was from Enzo Life Sciences.

Antisera. For Western blotting, 4G10 (05-321) was from Millipore; PKC substrate (6967), Akt substrate (9614), MAPK substrate (2325), PLCγ2 Y_{1217}, DAPP1 Y_{139} (13703), GSK3α S_{21} (9316), Hsp27 S_{82} (9709), FLNA S_{2152} (4761), Syk Y_{323} (2715), Syk $Y_{525/526}$ (2711), PKCδ Y_{311} (2055), p38 $pT_{180}Y_{182}$ (4511), STAT1 S_{727} (8826), PLCβ3 S_{1105} (2484), PAK2 $S_{192}S_{197}$ (2605), PKD $S_{738}S_{742}$ (2054), CTNND1 S_{252} (8477), Lyn Y_{507} (2731), mTOR S_{2448} (2971), ERK2 $T_{185}Y_{187}$ (9106) and Rab7 (9367) were from Cell Signaling; VASP S_{239} (sc-101439) was from Santa Cruz; GEFH1 S_{885} (ab94348) and Fyn Y_{530} (ab182661) were from Abcam; PDE3A S_{428} (S446B) was from MRC Protein Phosphorylation and Ubiquitylation Unit (Dundee); Tubulin (T6199) was from Sigma; STIM1 pS575 antibody was from F. J. Martin-Romero (U. Extremadura, Spain); RGS18 antisera were from A. Smolenski (Dublin). For human flow cytometry studies, FITC anti-human CD41a (HIP8), FITC anti-human PAC-1, BUV395 anti-human CD45 (HI30), PE-Cy7 anti-human CD14 (M5E2) were from BD Biosciences. BV421 anti-human CD41a (HIP8) and APC anti-human CD62P (AK4) were from BioLegend. For fluorescence microscopy, anti-Rab7 was from Abcam; anti-CD63 was from Santa Cruz.

Inhibitors. MRS 2179, AR-C 66096, PP2, Ro 31-8220, H89, SB202190, SB216763, CHIR 99021, Cariporide, Anagrelide, AZ PFKFB3 67, MLi-2, and (5Z)-7-Oxozeaenol were from Tocris. Entospletinib, Ibrutinib, Acalabrutinib, and LY3214996 were from Selleck. APS-2-79 was from Sigma. NSC-658497 was provided by Y. Zheng (Children's Hospital; Cincinnati, OH).

Platelet preparation

Washed human platelets were prepared from blood drawn from a rotating pool of healthy, adult (>18 y old) male and female volunteers by venipuncture into 1:10 sodium citrate (3.8%) in accordance with an Oregon Health & Science University IRB-approved protocol, as previously described.[3] For Condition #1 and Condition #2 proteomics studies, blood was drawn from 3 male and 2 female donors (n=5) from this same donor pool to prepare platelets. Platelets were resuspended in modified HEPES/Tyrode (H-T) buffer (129 mM NaCl, 0.34 mM Na_2HPO_4, 2.9 mM KCl, 12 mM $NaHCO_3$, 20 mM HEPES, 5 mM glucose, 1 mM $MgCl_2$; pH 7.3). Washed platelet preparations were routinely analyzed by flow cytometry (Figure S5) using a BD FACSymphony A5 Flow Cytometer to confirm sample purity (>99% CD41+; <0.01% CD45+; <0.01% CD235a+) and resting state (<5% CD62P+), as previously described.[4] This work was conducted in accordance with the Declaration of Helsinki.

Sample Preparation and Lysis

For proteomics studies, equivalent platelet suspensions (1×10^9/ml, 4 ml each in 15 ml Falcon tubes) in H-T buffer containing apyrase (2 U/ml), indomethacin (10 μM) and Integrilin (20 μg/ml) ("Condition #1") or Integrilin alone ("Condition #2") were left untreated or stimulated with 10 μg/ml CRP-XL (5 min, 37°C). Previous studies from our group and others have confirmed that these conditions allow for the study of a range of GPVI-driven signaling events in platelets.[5-9] These conditions also allow for precise and reproducible quantification of intracellular calcium signaling events in lieu of the variable effects of adding exogenous calcium, magnesium and trace levels of other divalent cations.[10] After 5 min, resting and activated platelet samples were resuspended in an equal volume of 2× lysis buffer (also warmed to 37°C; final buffer concentrations: 100 mM Tris-HCl pH 8, 65 mM NaCl, 10 mM HEPES, 6 mM $NaHCO_3$, 1.45 mM KCl, 0.5 mM $MgCl_2$, 0.17 mM Na_2HPO_4, 5 mM glucose, 0.5% sodium

deoxycholate, 1 mM NaF and 1 mM sodium orthovanadate, 1× Sigma Phosphatase Inhibitor Cocktail 2 & 3) and were immediately flash frozen in liquid nitrogen and stored at -80°C for later analysis. A small volume (50 µl) of each sample was prepared in Laemmli sample buffer for Western blot analysis. After thawing, lysates were further lysed by probe sonication (4× for 30 s with a 30 s rest between cycles, power 5-6). Protein concentrations were then determined using the Pierce BCA Protein Assay Kit (Thermo Scientific).

Sample digestion

Exact protein amounts per lysate sample digest and peptide used per sample enrichment are shown in "Full" detail tabs of Supplemental Table S1. Approximately 10-40 mg of protein per sample was reduced with 1/10 volume of 150 mM tris(2-carboxyethyl)phosphine (TCEP) at 55°C for 15 min (adjusted to pH~8 with NaOH), then alkylated with 1/100 volume of 500 mM iodoacetamide at room temperature in the dark for 60 min. Water was added to reduce the sodium deoxycholate concentration to 0.2%, then trypsin (97%, Worthington, Lakewood NJ) was added at a 25:1 protein:trypsin ratio. The samples were incubated overnight at 37°C before quenching with TFA (final concentration 1%). The samples were centrifuged at 3,000 × g for 15 min at room temperature to remove precipitated deoxycholic acid before solid phase extraction.

Peptide sample cleanup

Peptides were purified by solid phase extraction using Waters Sep-pak Vac 3 cc (500 mg) tC18 cartridges (Waters Corporation, Milford, MA). Briefly, the cartridges were conditioned 3× with 3 ml of ACN followed by 1× with 3 ml of 50% ACN/0.5% acetic acid, then equilibrated 3× with 3 ml of 0.1% TFA. The samples were loaded and passed through the bed, then were washed 3× with 3 ml of 0.1% TFA followed by 0.9 ml of 0.5% acetic acid. Finally, the samples were eluted with 5 ml of 50% ACN/0.5% acetic acid. Peptide concentrations were determined using the Pierce Quantitative Colorimetric Peptide Assay (Thermo Scientific, Rockford, IL). A portion of the digests for Condition #2 were used for whole proteome expression measurements. The peptide samples were lyophilized.

Immunoaffinity Purification (IAP)

A PTMScan P-Tyr-1000 Rabbit mAb kit (Cat. #8803) (Cell Signaling Technology, Danvers MA) was used to enrich tyrosine-phosphorylated peptides from the human platelet peptide samples prior to enrichment of phosphorylated peptides with TiO_2 beads (see below). For pTyr enrichment, 80 µl tubes of resin were split between two samples, such that each sample was enriched with 40 µl of antibody slurry. The antibody slurry was washed 3× with 0.5 ml of PBS (50 mM Na_2HPO_4, 150 mM NaCl) and once with 0.4 ml of IAP buffer. The peptides were resuspended in 1 ml of IAP buffer, and 40 µl of antibody slurry was added to each sample. Each peptide sample-antibody slurry mixture was rotated at 4°C for 2 hrs. After incubation, the flow-through was set aside for subsequent enrichments, and the slurry containing the enriched peptides was washed 2× with 0.5 ml of IAP buffer, 2× with 0.5 ml of water, and a final time with 0.4 ml of water. The enriched peptides were eluted from the antibody slurry with 2× 50 µl of 0.5-1% formic acid, with a 10 min incubation with agitation each time, before being purified by solid phase extraction.

Phosphopeptide enrichment with TiO_2 beads

The flow-through from the pTyr mAb enrichment was acidified to a final TFA concentration of 1%, and then solid phase extracted using Waters Sep-pak Vac 3 cc (500 mg) tC18 cartridges (see above). A peptide assay was then performed, and phosphopeptides were enriched using methods previously published.[11] Briefly, Titanosphere TiO_2 5 µm particles (GL Biosciences, Tokyo, Japan) were washed three times in 2 M lactic acid/50% ACN and resuspended in the same solution at a concentration of 0.33

mg/µl. Approximately 3-15 mg of dried peptide was resuspended in 900 µl of 2 M lactic acid/50% ACN, and the bead suspension was added to each sample, ensuring a 4:1 or 5:1 ratio of TiO_2 beads:peptide. The bead:peptide mixture was rotated at room temperature for 1 hr. The beads were then washed 2× with 500 µl of each solution: 2M lactic acid/50% ACN, 0.1% TFA/50% ACN, then 0.1% TFA/25% ACN. The enriched phosphopeptides were eluted from the beads by vortexing in 100 µl of 50 mM K_2HPO_4 pH 10 for 5 min. The elution step was repeated once for a total of 200 µl. The TiO_2 enriched phosphopeptide samples were acidified to a final TFA concentration of 2% before the sample cleanup step (see below).

Enriched peptide sample cleanup

The pTyr and TiO_2-enriched phosphopeptides were purified by solid phase extraction using Nest Group columns (The Nest Group, Inc., Southborough, MA). Spin columns included: UltraMicro Spin Column, MicroSpin Columns, MacroSpin Columns and BioPureSPN MIDI SPE; the choice of spin column varied depending on the amount of peptide in the sample. For Ab enriched samples, columns were conditioned with 50% ACN/0.1% TFA and equilibrated with 0.1% TFA. The samples were loaded and passed through the columns three times. The samples were washed with 0.1%TFA then eluted with 40% ACN/0.1% FA. The samples were dried down in preparation for TMT labeling. For TiO_2 enriched samples, columns were conditioned with 80% ACN/0.1% TFA and equilibrated with 0.1% TFA. The samples were loaded and passed through the columns three times. The samples were washed with 0.1%TFA then eluted with 80% ACN/0.1% FA. The samples were dried down in preparation for TMT labeling.

TMT labeling

TMT 10-plex reagents were each dissolved in anhydrous ACN. The peptides were reconstituted in 100 mM triethylammonium bicarbonate (TEAB) and added to 0.200 mg of its respective 10-plex TMT reagent, except for Condition 1 experiments, where 0.133 mg of TMT reagent was used to label the pTyr enriched peptides. The samples were incubated for 1 hour at room temperature with gentle mixing. Reaction mixtures (2 µl each) were then pooled, 2 µl of 5% hydroxylamine added, and the combined sample incubated for a further 15 min with gentle mixing. The mixture was then dried down, dissolved in 5% formic acid, and the phosphopeptides analyzed by a single 2-hour LC-MS/MS method using an Orbitrap Fusion as described below. This run was performed to normalize the total reporter ion intensity of each multiplexed sample and to check TMT labeling efficiency. The remaining samples were quenched by addition of 2 µl of 5% hydroxylamine as above, then combined in an equal ratio based on total reporter ion intensities determined during the normalization run and dried down in preparation for 2D-LC-MS/MS analysis.

LC-MS/MS analysis

Multiplexed TMT-labeled samples were reconstituted in 10 mM ammonium formate pH 9 and separated by two-dimensional reverse-phase liquid chromatography using a Dionex NCS-3500RS UltiMate RSLCnano UPLC system. The 20-40 µl reconstituted samples were injected onto a NanoEase 5 µm XBridge BEH130 C18 300 µm x 50 mm column (Waters) at 3 µl/min in a mobile phase containing 10 mM ammonium formate (pH 9). Peptides were eluted by sequential injection of 20 µl volumes of 4, 6, 8, 10, 12, 14, 16, 18, 20, 22, 25, 30, and 60% ACN in 10 mM ammonium formate (pH 9) at 3 µl/min flow rate. (For the "Condition 2" TiO2 enriched peptide sample, the fractions were: 4, 6, 8, 10, 11, 12, 13, 14, 15, 16, 17, 18, 19, 20, 22, 25, 30, and 60% ACN). For the Condition #2 whole proteome peptide sample, the fractions were: 14, 17, 20, 21, 22, 23, 24, 25, 26, 27, 28, 29, 30, 35, 40, 45, 50, and 90% ACN. Eluted peptides from the first-dimension column were diluted with mobile phase containing 0.1% formic acid at 24 µl/min flow rate and delivered to an Acclaim PepMap 100 µm x 2 cm NanoViper C18, 5 µm trap on a switching valve. After 10 min of loading, the trap column was switched on-line to a PepMap

RSLC C18, 2 µm, 75 µm x 25 cm EasySpray column (Thermo Scientific). Peptides were then separated at low pH in the second dimension using a 7.5–30% ACN gradient over 90 min in mobile phase containing 0.1% formic acid at 300 nL/min flow rate. Each second-dimension LC run required 2 h for separation and re-equilibration, so each 2D LC-MS/MS method required 26-36 h for completion, depending if 13 or 18 fractions were used. Tandem mass spectrometry data was collected using an Orbitrap Fusion Tribrid instrument (Thermo Scientific) configured with an EasySpray NanoSource (Thermo Scientific). Survey scans were performed in the Orbitrap mass analyzer (resolution = 120,000), and data-dependent MS2 scans performed in the linear ion trap using collision-induced dissociation (normalized collision energy = 35) following isolation with the instrument's quadrupole. Reporter ion detection was performed in the Orbitrap mass analyzer (resolution = 60,000) using MS3 scans following synchronous precursor scan isolation (SPS) of the top 10 ions in the quadrupole, and higher-energy collisional dissociation in the ion-routing multipole (normalized collision energy = 65).

MS Data Analysis

RAW instrument files for the phosphopeptide enrichment experiments were processed using Proteome Discoverer (PD) version 1.4.1.14 (Thermo Scientific). For each of the TMT experiments, raw files from the 13-18 fractions were merged and searched with the SEQUEST HT search engine. For Condition #1 experiments, a *Homo sapiens* UniProt Swiss-Prot protein database downloaded October 2016 (20,120 entries) was used; for Condition #2 experiments, a database downloaded January 2018 (21,008 sequences) was used. Searches were configured with static modifications for the TMT reagents (+229.1629 Da on peptide N-termini and lysines) and carbamidomethyl (+57.0215 Da) on cysteines; dynamic modifications for oxidation of methionine residues (+15.9949 Da; only for Condition #1) and phosphorylation (+79.9663) of serine, threonine and tyrosine residues; parent ion tolerance of 1.25 Da; fragment mass tolerance of 1.0005 Da; monoisotopic masses; and trypsin cleavage (max 2 missed cleavages). The phosphorylation site localization node phosphoRS was configured after the search node in Proteome Discoverer.[12] Searches used a reversed sequence decoy strategy to control peptide false discovery and identifications were validated by Percolator software. Only peptides with q scores ≤ 0.01 and parent ion mass deviations of less than 20 ppm were accepted. A maximum of 5 total modifications per peptide were allowed with a maximum of 3 phosphorylation sites per peptide.

A Python script (PD1.4_TMT_phospho_processer.py), available at https://github.com/pwilmart/PAW_pipeline was used for post-processing of the Proteome Discoverer exported peptide-spectrum match (PSM) results as previously described.[13] Summation of reporter ions from all PSMs having the same amino acid peptide sequence with the same total number and types of modifications was done to improve data quality and reduce the quantitative data set size. Summarized data was tested for differential expression using the Bioconductor R package edgeR and Jupyter notebooks.[14] Data was normalized with the trimmed mean of M-values (TMM) option and an exact test was used with Benjamini-Hochberg multiple testing corrections, as previously described.[13] Jupyter notebook files that work through normalization, statistical analyses and other data processing details are included in the Supplemental materials of this manuscript as html files and are also deposited in the ProteomeXchange PRIDE partner archive associated with this project (dataset identifier PXD017167). For visualization, datasets were additionally analyzed with the START app.[15]

The whole proteome expression study used the PAW/Comet pipeline.[16,17] Search parameters were similar to those above; variable modifications included oxidized methionine but did not include phosphorylation. Accurate masses and target/decoy score distributions were used to filter PSMs to a false discovery rate of 1%. Protein inference used basic and extended parsimony logic, and a minimum of two peptides per protein. Whole protein differential expression analysis was performed with edgeR similar to the above description, and as previously described.[18-26] Jupyter notebook files that narratively walk through data processing and analysis details are included in the Supplemental materials of this manuscript as html files and are also deposited in the ProteomeXchange PRIDE partner archive

associated with this project (dataset identifier PXD017167). Additional UniProt annotations were added to results tables using Python scripts available at https://github.com/pwilmart/annotations.

Platelet adhesion and spreading assays

For platelet adhesion and spreading experiments, 12 mm #1.5 glass coverslips (Fisher Scientific) or cover glass bottom dishes (MatTek) were coated with CRP-XL (2 μg/ml) or human fibrinogen (50 μg/ml), followed by surface blocking with denatured, filtered, fatty acid-free BSA (5 mg/ml). Vehicle (0.1% DMSO) or inhibitors were added to platelets in solution (2×10^7/ml) for 10 min prior to seeding on immobilized surfaces. After 45 min at 37°C, adherent platelets were washed (3×, PBS). Adherent platelets were then fixed with 4% paraformaldehyde (PFA) in PBS at room temperature for 10 min prior to three additional PBS washes and mounting on glass slides with Fluoromount G (Southern Biotech). Platelets were imaged using Kohler-illuminated Nomarski differential interference contrast (DIC) optics with a Zeiss 63× oil immersion 1.40 NA plan-apochromat lens on a Zeiss Axio Imager M2 microscope using Slidebook 5.5 image acquisition software (Intelligent Imaging Innovations) as described.[3]

Fluorescence microscopy

Following fixation (4% PFA), platelets were incubated with poly-l-lysine coated cover glass dishes (MatTek) for 30 min, prior to washing with PBS and permeabilization with a blocking solution (1% Fraction V BSA and 0.1% SDS in PBS), as previously described.[27] Platelets were then stained with indicated primary antibodies overnight at 4°C at a 1:100-500 dilution in blocking buffer. Alexa Fluor secondary antibodies (1:100-500) or TRITC-phalloidin (1:500) were added in blocking buffer (2 h). After washing with PBS, platelet samples were coated with Fluoromount G. Platelets were imaged with lattice-based super resolution structured illumination microscopy (SR-SIM) with a Zeiss 63× oil immersion 1.4 NA plan-apochromat lens on a Zeiss Elyra 7 microscope. Raw data was processed using Zeiss Zen software-suggested automated filter settings.

Dense granule (ADP) secretion assays

Platelet dense granule (i.e., ADP) secretion was measured as the light output generated by an ATP-luciferin-luciferase reaction as previously described.[28] Briefly, human washed platelets (2×10^8/ml) were incubated with inhibitors (as indicated) or vehicle alone (0.1% DMSO, 10 min, 37°C). Platelets were then incubated with orbital shaking in a white, flat bottom 96-well plate (Corning Costar) in the presence of platelet agonist for 30 sec at 37°C. Detection reagent Chrono-lume (Chrono-Log Corporation) was added to the wells and sample luminescence was measured with an Infinite M200 spectrophotometer (TECAN). A grouped analysis was performed to determine statistical significance using two-way ANOVA with post hoc Tukey's comparison test in GraphPad PRISM 8.

Platelet α-granule secretion, integrin activation and F-actin content

Flow cytometry assays of platelet α-granule secretion, integrin activation and F-actin content were carried out as previously described.[8] Briefly, washed human platelets (2×10^8/ml) were preincubated with vehicle (0.1% DMSO) or inhibitors, as indicated, for 10 min at 37°C and then stimulated with CRP-XL for 30 min in the presence of FITC-conjugated anti-human PAC-1 or APC-conjugated anti-human CD62P antibodies. For F-actin content measurements, parallel platelet samples were incubated in the absence of labeling antibodies, and were fixed after 30 min CRP-XL stimulation with 2% PFA prior to permeabilization and staining with FITC-phalloidin. Samples were diluted in H-T buffer and then analyzed on a FACSCanto II system, as previously described.[8] Mean fluorescence intensity (MFI) measurements and percentages of positive, antibody labeled (CD41+) platelet-gated events were analyzed by for statistical significance by one-way ANOVA using GraphPad PRISM 8.

Platelet aggregation and thromboxane generation

Washed platelets in H-T buffer (2×10^8/ml, 300 µl per sample) were preincubated in glass cuvettes and warmed to 37°C in the absence or presence of apyrase, indomethacin, Integrilin or other agents, as detailed. Platelet aggregation under stirring conditions was initiated by CRP-XL (10 µg/ml), and changes in light transmission were monitored for 5 minutes using a PAP-4 aggregometer (Chrono-Log Corporation). After 5 min, solutions were removed from cuvettes and cleared by centrifugation prior to analysis for TXB2 content by ELISA assay. Percentages of platelet aggregation relative to positive control and measured TBX2 concentrations were analyzed for statistical significance by one-way ANOVA testing for multiple comparisons using GraphPad PRISM 8 software.

Western blot, Phos-tag gel electrophoresis

Western blots were performed as previously described.[29] For Phos-tag gel separation of phosphorylated Rab7, 10% PAGE gels were supplemented with 25 µM Phos-tag acrylamide and 50 µM $MnCl_2$, as previously described.[30] Following blot development, band densitometry measurements were performed in Image J and data were analyzed by ANOVA test for trend (Figure 1F) or one-way ANOVA with post hoc Tukey's comparison test (Figure 5A) For comparisons of effects of apyrase and indomethacin protein (de)phosphorylation in response to CRP-XL (Figure 2G, 3G), blot intensities were analyzed with paired t-test. Statistical analyses were performed using GraphPad PRISM 8.

Gene ontology (GO), Reactome and Interactome analysis

Lists of low, medium and high confidence (FDR<0.1) candidate proteins from Table S1 with significantly differential phosphorylation from Condition #1 and #2 experiments were queried for Gene Ontology (GO) Biological Process and Molecular Function terms through STRING (v11.0) or The Gene Ontology Resource.[31,32] For interactome analysis, a total of 3,723 platelet proteins identified in our study were examined for interactive relations with Cytoscape using stringApp and further grouped by using ReactomeFIPlugIn. Sets of proteins with significant phosphorylation changes were also queried with Reactome.[33] Results of analyses are available in Supplemental Table S3.

Pathway analysis

We used CausalPath to identify the pathway fragments that can directly explain correlated changes in phosphoproteomic datasets.[29,34] CausalPath first processes the Pathway Commons database[35] using the BioPAX-pattern library,[36] searching for graphical patterns that capture potential binary cause-effect relations between protein activities, abundances and modifications.[34] CausalPath then selects the subset of the causal relations that fit the given data. In addition to Pathway Commons data, we performed a manual literature curation for some of the phosphorylation site effects that were not covered by Pathway Commons. We used CausalPath in two modes: (i) default mode; and (ii) by relaxing site-matching constraints by 1 amino acid difference. The site-matching constraint requires the phosphorylation site position to be mentioned in the pathway model, and to exactly match with the site position identified and measured in the phosphoproteomics dataset of interest. Allowing one amino acid difference in the site position is a workaround for covering the inconsistencies in the curation of site positions in pathway databases. CausalPath is available at *https://github.com/PathwayAndDataAnalysis/causalpath*. CausalPath result networks are rendered with the ChiBE visualization tool[37,38] which is available at *https://github.com/PathwayCommons/chibe*

Supplemental References

1. Perez-Riverol Y, Csordas A, Bai J, et al. The PRIDE database and related tools and resources in 2019: improving support for quantification data. *Nucleic Acids Res*. 2019;47(D1):D442-D450.
2. Sari M, Bahceci I, Dogrusoz U, et al. SBGNViz: A Tool for Visualization and Complexity Management of SBGN Process Description Maps. *PLoS One*. 2015;10(6):e0128985.
3. Aslan JE, Itakura A, Gertz JM, McCarty OJ. Platelet shape change and spreading. *Methods Mol Biol*. 2012;788:91-100.
4. Mitrugno A, Tassi Yunga S, Sylman JL, et al. The role of coagulation and platelets in colon cancer-associated thrombosis. *Am J Physiol Cell Physiol*. 2019;316(2):C264-C273.
5. Aslan JE, Baker SM, Loren CP, et al. The PAK system links Rho GTPase signaling to thrombin-mediated platelet activation. *Am J Physiol Cell Physiol*. 2013;305(5):C519-528.
6. Loren CP, Aslan JE, Rigg RA, et al. The BCR-ABL inhibitor ponatinib inhibits platelet immunoreceptor tyrosine-based activation motif (ITAM) signaling, platelet activation and aggregate formation under shear. *Thromb Res*. 2015;135(1):155-160.
7. White TC, Berny MA, Robinson DK, et al. The leech product saratin is a potent inhibitor of platelet integrin alpha2beta1 and von Willebrand factor binding to collagen. *FEBS J*. 2007;274(6):1481-1491.
8. Aslan JE, Itakura A, Haley KM, et al. p21 activated kinase signaling coordinates glycoprotein receptor VI-mediated platelet aggregation, lamellipodia formation, and aggregate stability under shear. *Arterioscler Thromb Vasc Biol*. 2013;33(7):1544-1551.
9. Rigg RA, Aslan JE, Healy LD, et al. Oral administration of Bruton's tyrosine kinase inhibitors impairs GPVI-mediated platelet function. *Am J Physiol Cell Physiol*. 2016;310(5):C373-380.
10. Watson SP, Poole A, Asselin J. Ethylene glycol bis(beta-aminoethyl ether)-N,N,N',N'-tetraacetic acid (EGTA) and the tyrphostin ST271 inhibit phospholipase C in human platelets by preventing Ca2+ entry. *Mol Pharmacol*. 1995;47(4):823-830.
11. Kettenbach AN, Gerber SA. Rapid and reproducible single-stage phosphopeptide enrichment of complex peptide mixtures: application to general and phosphotyrosine-specific phosphoproteomics experiments. *Anal Chem*. 2011;83(20):7635-7644.
12. Taus T, Kocher T, Pichler P, et al. Universal and confident phosphorylation site localization using phosphoRS. *J Proteome Res*. 2011;10(12):5354-5362.
13. Wakeham CM, Wilmarth PA, Cunliffe JM, et al. Identification of PKCalpha-dependent phosphoproteins in mouse retina. *J Proteomics*. 2019;206:103423.
14. Robinson MD, McCarthy DJ, Smyth GK. edgeR: a Bioconductor package for differential expression analysis of digital gene expression data. *Bioinformatics*. 2010;26(1):139-140.
15. Nelson JW, Sklenar J, Barnes AP, Minnier J. The START App: a web-based RNAseq analysis and visualization resource. *Bioinformatics*. 2017;33(3):447-449.
16. Wilmarth PA, Riviere MA, David LL. Techniques for accurate protein identification in shotgun proteomic studies of human, mouse, bovine, and chicken lenses. *J Ocul Biol Dis Infor*. 2009;2(4):223-234.
17. Eng JK, Jahan TA, Hoopmann MR. Comet: an open-source MS/MS sequence database search tool. *Proteomics*. 2013;13(1):22-24.
18. Abdelhamed S, Butler JT, Doron B, et al. Extracellular vesicles impose quiescence on residual hematopoietic stem cells in the leukemic niche. *EMBO Rep*. 2019;20(7):e47546.
19. Hegarty DM, David LL, Aicher SA. Lacrimal Gland Denervation Alters Tear Protein Composition and Impairs Ipsilateral Eye Closures and Corneal Nociception. *Invest Ophthalmol Vis Sci*. 2018;59(12):5217-5224.
20. Huan J, Hornick NI, Goloviznina NA, et al. Coordinate regulation of residual bone marrow function by paracrine trafficking of AML exosomes. *Leukemia*. 2015;29(12):2285-2295.
21. Hulett TW, Jensen SM, Wilmarth PA, et al. Coordinated responses to individual tumor antigens by IgG antibody and CD8+ T cells following cancer vaccination. *J Immunother Cancer*. 2018;6(1):27.
22. Krey JF, Dumont RA, Wilmarth PA, David LL, Johnson KR, Barr-Gillespie PG. ELMOD1 Stimulates ARF6-GTP Hydrolysis to Stabilize Apical Structures in Developing Vestibular Hair Cells. *J Neurosci*. 2018;38(4):843-857.

23. Plubell DL, Fenton AM, Wilmarth PA, et al. GM-CSF driven myeloid cells in adipose tissue link weight gain and insulin resistance via formation of 2-aminoadipate. *Sci Rep*. 2018;8(1):11485.
24. Plubell DL, Wilmarth PA, Zhao Y, et al. Extended Multiplexing of Tandem Mass Tags (TMT) Labeling Reveals Age and High Fat Diet Specific Proteome Changes in Mouse Epididymal Adipose Tissue. *Mol Cell Proteomics*. 2017;16(5):873-890.
25. Svensson K, LaBarge SA, Sathe A, et al. p300 and cAMP response element-binding protein-binding protein in skeletal muscle homeostasis, contractile function, and survival. *J Cachexia Sarcopenia Muscle*. 2020;11(2):464-477.
26. Vranka JA, Staverosky JA, Reddy AP, et al. Biomechanical Rigidity and Quantitative Proteomics Analysis of Segmental Regions of the Trabecular Meshwork at Physiologic and Elevated Pressures. *Invest Ophthalmol Vis Sci*. 2018;59(1):246-259.
27. Ngo AT, Thierheimer ML, Babur O, et al. Assessment of roles for the Rho-specific guanine nucleotide dissociation inhibitor Ly-GDI in platelet function: a spatial systems approach. *Am J Physiol Cell Physiol*. 2017;312(4):C527-C536.
28. Mitrugno A, Rigg RA, Laschober NB, et al. Potentiation of TRAP-6-induced platelet dense granule release by blockade of P2Y12 signaling with MRS2395. *Platelets*. 2017:1-12.
29. Babur O, Ngo ATP, Rigg RA, et al. Platelet procoagulant phenotype is modulated by a p38 - MK2 axis regulating RTN4/Nogo proximal to the endoplasmic reticulum: utility of pathway analysis. *Am J Physiol Cell Physiol*. 2018.
30. Kinoshita E, Kinoshita-Kikuta E, Takiyama K, Koike T. Phosphate-binding tag, a new tool to visualize phosphorylated proteins. *Mol Cell Proteomics*. 2006;5(4):749-757.
31. The Gene Ontology C. The Gene Ontology Resource: 20 years and still GOing strong. *Nucleic Acids Res*. 2019;47(D1):D330-D338.
32. Ashburner M, Ball CA, Blake JA, et al. Gene ontology: tool for the unification of biology. The Gene Ontology Consortium. *Nat Genet*. 2000;25(1):25-29.
33. Jassal B, Matthews L, Viteri G, et al. The reactome pathway knowledgebase. *Nucleic Acids Res*. 2020;48(D1):D498-D503.
34. Babur O, Luna A, Korkut A, et al. Causal interactions from proteomic profiles: molecular data meets pathway knowledge. *bioRxiv*. 2018.
35. Cerami EG, Gross BE, Demir E, et al. Pathway Commons, a web resource for biological pathway data. *Nucleic Acids Res*. 2011;39(Database issue):D685-690.
36. Babur O, Aksoy BA, Rodchenkov I, Sumer SO, Sander C, Demir E. Pattern search in BioPAX models. *Bioinformatics*. 2014;30(1):139-140.
37. Babur O, Dogrusoz U, Cakir M, et al. Integrating biological pathways and genomic profiles with ChiBE 2. *BMC Genomics*. 2014;15:642.
38. Babur O, Dogrusoz U, Demir E, Sander C. ChiBE: interactive visualization and manipulation of BioPAX pathway models. *Bioinformatics*. 2010;26(3):429-431.
39. Carrim N, Walsh TG, Consonni A, Torti M, Berndt MC, Metharom P. Role of focal adhesion tyrosine kinases in GPVI-dependent platelet activation and reactive oxygen species formation. *PLoS One*. 2014;9(11):e113679.
40. Murugappan S, Shankar H, Bhamidipati S, Dorsam RT, Jin J, Kunapuli SP. Molecular mechanism and functional implications of thrombin-mediated tyrosine phosphorylation of PKCdelta in platelets. *Blood*. 2005;106(2):550-557.
41. Cicmil M, Thomas JM, Sage T, et al. Collagen, convulxin, and thrombin stimulate aggregation-independent tyrosine phosphorylation of CD31 in platelets. Evidence for the involvement of Src family kinases. *J Biol Chem*. 2000;275(35):27339-27347.
42. Dorsam RT, Kim S, Murugappan S, et al. Differential requirements for calcium and Src family kinases in platelet GPIIb/IIIa activation and thromboxane generation downstream of different G-protein pathways. *Blood*. 2005;105(7):2749-2756.
43. Palumbo R, De Marchis F, Pusterla T, Conti A, Alessio M, Bianchi ME. Src family kinases are necessary for cell migration induced by extracellular HMGB1. *J Leukoc Biol*. 2009;86(3):617-623.

44. Bain J, McLauchlan H, Elliott M, Cohen P. The specificities of protein kinase inhibitors: an update. *Biochem J*. 2003;371(Pt 1):199-204.
45. Brandvold KR, Steffey ME, Fox CC, Soellner MB. Development of a highly selective c-Src kinase inhibitor. *ACS Chem Biol*. 2012;7(8):1393-1398.
46. Tummler C, Dumitriu G, Wickstrom M, et al. SYK Inhibition Potentiates the Effect of Chemotherapeutic Drugs on Neuroblastoma Cells in Vitro. *Cancers (Basel)*. 2019;11(2).
47. Sun H, Lin DC, Cao Q, et al. Identification of a Novel SYK/c-MYC/MALAT1 Signaling Pathway and Its Potential Therapeutic Value in Ewing Sarcoma. *Clin Cancer Res*. 2017;23(15):4376-4387.
48. Currie KS, Kropf JE, Lee T, et al. Discovery of GS-9973, a selective and orally efficacious inhibitor of spleen tyrosine kinase. *J Med Chem*. 2014;57(9):3856-3873.
49. Sharman J, Hawkins M, Kolibaba K, et al. An open-label phase 2 trial of entospletinib (GS-9973), a selective spleen tyrosine kinase inhibitor, in chronic lymphocytic leukemia. *Blood*. 2015;125(15):2336-2343.
50. Nicolson PLR, Hughes CE, Watson S, et al. Inhibition of Btk by Btk-specific concentrations of ibrutinib and acalabrutinib delays but does not block platelet aggregation mediated by glycoprotein VI. *Haematologica*. 2018;103(12):2097-2108.
51. Series J, Garcia C, Levade M, et al. Differences and similarities in the effects of ibrutinib and acalabrutinib on platelet functions. *Haematologica*. 2019;104(11):2292-2299.
52. Nicolson PLR, Nock SH, Hinds J, et al. Low dose Btk inhibitors selectively block platelet activation by CLEC-2. *Haematologica*. 2020.
53. Byrd JC, Harrington B, O'Brien S, et al. Acalabrutinib (ACP-196) in Relapsed Chronic Lymphocytic Leukemia. *N Engl J Med*. 2016;374(4):323-332.
54. Levade M, David E, Garcia C, et al. Ibrutinib treatment affects collagen and von Willebrand factor-dependent platelet functions. *Blood*. 2014;124(26):3991-3995.
55. Ninomoto J, Mokatrin A, Kinoshita T, et al. Effects of ibrutinib on in vitro platelet aggregation in blood samples from healthy donors and donors with platelet dysfunction. *Hematology*. 2020;25(1):112-117.
56. Honigberg LA, Smith AM, Sirisawad M, et al. The Bruton tyrosine kinase inhibitor PCI-32765 blocks B-cell activation and is efficacious in models of autoimmune disease and B-cell malignancy. *Proc Natl Acad Sci U S A*. 2010;107(29):13075-13080.
57. Pears CJ, Thornber K, Auger JM, et al. Differential roles of the PKC novel isoforms, PKCdelta and PKCepsilon, in mouse and human platelets. *PLoS One*. 2008;3(11):e3793.
58. Paul BZ, Jin J, Kunapuli SP. Molecular mechanism of thromboxane A(2)-induced platelet aggregation. Essential role for p2t(ac) and alpha(2a) receptors. *J Biol Chem*. 1999;274(41):29108-29114.
59. Zhao L, Liu J, He C, et al. Protein kinase A determines platelet life span and survival by regulating apoptosis. *J Clin Invest*. 2017;127(12):4338-4351.
60. Lochner A, Moolman JA. The many faces of H89: a review. *Cardiovasc Drug Rev*. 2006;24(3-4):261-274.
61. Gambaryan S, Kobsar A, Rukoyatkina N, et al. Thrombin and collagen induce a feedback inhibitory signaling pathway in platelets involving dissociation of the catalytic subunit of protein kinase A from an NFkappaB-IkappaB complex. *J Biol Chem*. 2010;285(24):18352-18363.
62. Li D, August S, Woulfe DS. GSK3beta is a negative regulator of platelet function and thrombosis. *Blood*. 2008;111(7):3522-3530.
63. Moore SF, van den Bosch MT, Hunter RW, Sakamoto K, Poole AW, Hers I. Dual regulation of glycogen synthase kinase 3 (GSK3)alpha/beta by protein kinase C (PKC)alpha and Akt promotes thrombin-mediated integrin alphaIIbbeta3 activation and granule secretion in platelets. *J Biol Chem*. 2013;288(6):3918-3928.
64. Davies SP, Reddy H, Caivano M, Cohen P. Specificity and mechanism of action of some commonly used protein kinase inhibitors. *Biochem J*. 2000;351(Pt 1):95-105.
65. Li Z, Zhang G, Feil R, Han J, Du X. Sequential activation of p38 and ERK pathways by cGMP-dependent protein kinase leading to activation of the platelet integrin alphaIIb beta3. *Blood*. 2006;107(3):965-972.
66. Walsh TG, Berndt MC, Carrim N, Cowman J, Kenny D, Metharom P. The role of Nox1 and Nox2 in GPVI-dependent platelet activation and thrombus formation. *Redox Biol*. 2014;2:178-186.

67. Bhagwat SV, McMillen WT, Cai S, et al. ERK Inhibitor LY3214996 Targets ERK Pathway-Driven Cancers: A Therapeutic Approach Toward Precision Medicine. *Mol Cancer Ther*. 2020;19(2):325-336.
68. Che G, Gao H, Hu Q, Xie H, Zhang Y. Angiotensin II promotes podocyte injury by activating Arf6-Erk1/2-Nox4 signaling pathway. *PLoS One*. 2020;15(3):e0229747.
69. Purlyte E, Dhekne HS, Sarhan AR, et al. Rab29 activation of the Parkinson's disease-associated LRRK2 kinase. *EMBO J*. 2018;37(1):1-18.
70. Fell MJ, Mirescu C, Basu K, et al. MLi-2, a Potent, Selective, and Centrally Active Compound for Exploring the Therapeutic Potential and Safety of LRRK2 Kinase Inhibition. *J Pharmacol Exp Ther*. 2015;355(3):397-409.
71. Steger M, Diez F, Dhekne HS, et al. Systematic proteomic analysis of LRRK2-mediated Rab GTPase phosphorylation establishes a connection to ciliogenesis. *Elife*. 2017;6.
72. Kojok K, Akoum SE, Mohsen M, Mourad W, Merhi Y. CD40L Priming of Platelets via NF-kappaB Activation is CD40- and TAK1-Dependent. *J Am Heart Assoc*. 2018;7(23):e03677.
73. Hilt ZT, Pariser DN, Ture SK, et al. Platelet-derived beta2M regulates monocyte inflammatory responses. *JCI Insight*. 2019;4(5).
74. Acuna UM, Wittwer J, Ayers S, Pearce CJ, Oberlies NH, EJ DEB. Effects of (5Z)-7-oxozeaenol on the oxidative pathway of cancer cells. *Anticancer Res*. 2012;32(7):2665-2671.
75. Dhawan NS, Scopton AP, Dar AC. Small molecule stabilization of the KSR inactive state antagonizes oncogenic Ras signalling. *Nature*. 2016;537(7618):112-116.
76. Evelyn CR, Duan X, Biesiada J, Seibel WL, Meller J, Zheng Y. Rational design of small molecule inhibitors targeting the Ras GEF, SOS1. *Chem Biol*. 2014;21(12):1618-1628.
77. Chang HB, Gao X, Nepomuceno R, Hu S, Sun D. Na(+)/H(+) exchanger in the regulation of platelet activation and paradoxical effects of cariporide. *Exp Neurol*. 2015;272:11-16.
78. Teshima Y, Akao M, Jones SP, Marban E. Cariporide (HOE642), a selective Na+-H+ exchange inhibitor, inhibits the mitochondrial death pathway. *Circulation*. 2003;108(18):2275-2281.
79. Lim H, He D, Qiu Y, Krawczuk P, Sun X, Xie L. Rational discovery of dual-indication multi-target PDE/Kinase inhibitor for precision anti-cancer therapy using structural systems pharmacology. *PLoS Comput Biol*. 2019;15(6):e1006619.
80. Clark WF, Reid BD, Tevaarwerk GJ. Anagrelide: inhibitor of collagen and forming immune complex induced platelet aggregation and release. *Thromb Res*. 1981;21(1-2):215-219.
81. Clem BF, O'Neal J, Tapolsky G, et al. Targeting 6-phosphofructo-2-kinase (PFKFB3) as a therapeutic strategy against cancer. *Mol Cancer Ther*. 2013;12(8):1461-1470.
82. Boyd S, Brookfield JL, Critchlow SE, et al. Structure-Based Design of Potent and Selective Inhibitors of the Metabolic Kinase PFKFB3. *J Med Chem*. 2015;58(8):3611-3625.
83. Zheng X, Han H, Liu GP, et al. LncRNA wires up Hippo and Hedgehog signaling to reprogramme glucose metabolism. *EMBO J*. 2017;36(22):3325-3335.
84. MacKintosh C, MacKintosh RW. Inhibitors of protein kinases and phosphatases. *Trends Biochem Sci*. 1994;19(11):444-448.
85. Aslan JE. Platelet shape change. In: Gresele P, López J, Kleiman N, Page C, eds. Platelets in Thrombotic and Non-Thrombotic Disorders: Springer; 2017.
86. Aslan JE. Platelet Rho GTPase regulation in physiology and disease. *Platelets*. 2019;30(1):17-22.
87. Aslan JE, McCarty OJ. Rho GTPases in platelet function. *J Thromb Haemost*. 2013;11(1):35-46.
88. Estevez B, Du X. New Concepts and Mechanisms of Platelet Activation Signaling. *Physiology (Bethesda)*. 2017;32(2):162-177.
89. Li Z, Delaney MK, O'Brien KA, Du X. Signaling during platelet adhesion and activation. *Arterioscler Thromb Vasc Biol*. 2010;30(12):2341-2349.
90. Watson SP, Auger JM, McCarty OJ, Pearce AC. GPVI and integrin alphaIIb beta3 signaling in platelets. *J Thromb Haemost*. 2005;3(8):1752-1762.
91. Watson SP, Herbert JM, Pollitt AY. GPVI and CLEC-2 in hemostasis and vascular integrity. *J Thromb Haemost*. 2010;8(7):1456-1467.

Supplemental Notebooks

This manuscript includes Supplemental Notebooks as five html files that can be opened with any standard web browser (i.e., Chrome, Firefox). These html notebooks were prepared from Jupyter notebook files to detail proteomics data, normalization and statistical analyses associated with the above manuscript. The PRIDE partner repository archive associated with this manuscript (Project accession: PXD017167) also contains these notebooks (ipynb notebook files), their input data files, output files, and the notebooks rendered as HTML files, as well as R scripts with all of the content from the code cells.

Supplemental Tables

Table S1. Peptide identification and quantification details for Condition #1 and #2 experiments. An associated Supplemental Table and multi-tab .xls file contains raw data, MS3 TMT-labeled reporter ion intensity values, statistical analyses and other details for phosphopeptides identified and quantified in 5 separate human platelet samples under resting and +CRP-XL conditions (10 samples total per tab). Each tab lists (brief of "full") MS results for anti-pTyr- and TiO2-enriched samples under Condition #1 or Condition #2. Please see Manuscript and Supplemental Information and Table S1 “ReadMe” tab for additional details.

Table S2. Gene Ontology term and Reactome Pathway enrichment results. ***Related to Figure 3.*** An associated multi-tab .xls file contains full results of Gene Ontology (GO) term and Reactome pathway enrichment of candidate differentially phosphorylated proteins in Conditions #1 and #2.

Supplemental Table S3. ***Related to Figures 5, 6 and S14.*** **Specificities and other details of small molecule inhibitors used in this study.**

Abbrev.	Name(s)	Primary target(s)	IC50[a]	Other targets[b]	Established working concentrations[c]	Other notes	Refs
PP2	PP2	SFKs (Lck, Fyn)	4, 5 nM	Lck, EPH-B1, EPH-B3, CSK, EPH-B4, Src, EPH-A4, RIPK2, BTK, CK1, YES, HER4. FGF-R1	10 μM (Platelets, PMBCs and other cells)	• Non-specific SFK inhibitor regularly used to inhibit SFK activities in platelets at 10 μM	39-45
Ento	Entospletinib (GS-9973)	Syk	7.6 nM	BLK, MAP3K12, FLT3, HCK, KIT, LCK, LTK, MERTK, MLK1, PDGFRB RIOK, SRPK1, TNK1, TYK2	1-10 μM (Cancer cells)	• Highly selective, clinically relevant Syk inhibitor	46-49
Acal	Acalabrutinib	BTK	3 nM	BMX, ERBB4, TEC	1-10 μM (Platelets)	•Minimal off-target effects in platelets at 200 μM •Less potent, more selective BTK inhibitor	50-53
Ibru	Ibrutinib	BTK	0.5 nM	VEGFR1, RIPK2, CSK, HER4, Src, BRK, Lck, TIE2, Aurora A, EPH-B2, YES1, TrkA, Aurora B, FGF-R1BLK, BMX, FGR, BRK, HCK, EGFR, ERBB2, ITK	0.5-10 μM (Platelets and other cells)	• *Not used in signaling experiments in Fig. 5A* • Does not significantly inhibit non-BTK platelet responses at 10 μM	54-56
Ro	Ro 31-8220 (Bisindolylmaleimide IX)	PKCα/β	5 -24 nM	CLK2, MSK1, RSK2, TrkA, PIM3, PRK2, GSK3, Akt, IGF-1R, SGK, S6K, VEGFR1, RSK, MINK, SmMLCK, MLK3, PIM, NUAK, CAMKK, JAK2, SYK	5-20 μM (Platelets and other cells)	• Non-selective pan-PKC inhibitor. • Inhibits PKC-mediated platelet functions downstream of GPVI	57,58
H-89	H-89	PKA	135 nM	S6K1, NUAK1, Akt, MSK1, ROCK2, PRK2, RSK1, STK33, VEGFR1, ERK8, CHK2, AMPK, DYRK3	5-20 μM (Platelets)	• No off-target effect in platelets at 12.5 μM	59-61
SB2	SB216763	GSK3α/β	34.3 nM	ERK8, DYRK1A, SRPK1, HIPK2	10 μM (Platelets)	• High specificity GSK3 inhibitor	62
CHIR	CHIR 99021	GSK3β/α	6.7-10 nM	*No significant off-target inhibition*	1-10 μM (Platelets)	• Very high specificity GSK3 inhibitor	63
SB	SB202190	p38	38 nM	*No significant off-target inhibition*	1-10 μM (Platelets)	• *Used at 2 μM in studies in Fig. 5*	64-66
LY	LY3214996	ERK1/2	5 nM	Negligible off-target effects in cells found for: PIP5K3, MPSK1, GSK3, JNK, MPSK1, PKD1/2, NEK3	1-5 μM (Cell lines)	• Orally active, clinically relevant ERK1/2 inhibitor	67,68
MLi2	MLi2	LRRK2	0.76-3.4 nM	CLK2, TSSK1, NUAK1, JNK3, ASK1, CAMK1	0.1-1 μM (Cell lines)	• High specificity LRRK2 inhibitor • *Used at 1 μM in this study*	69-71
(5Z)-7	(5Z)-7-Oxozeaenol	TAK1	8 nM	MKK1, MKK2, ERK8, MKK6, MNK1, VEGFR1, PRAK, TrkA	0.1-10 μM (Platelets and cells)		72-74
APS	APS-2-79	KSR1	120 nM	BLK, EGFR, ERBB4, FGR, FYN, HCK, LCK, LYN, MERTK	0.5-5 μM (Cell lines)		75
NSC	NSC-658497	SOS1	15.4 μM	Not reported	20-100 μM (Cell lines)		76
Car	Cariporide (HOE 642)	NHE1, NHE3	0.05-3 μM	Not reported	10 μM (Platelets and other cells)	Reported antiplatelet agent, but effects on platelet activation are not clear	77,78
Ana	Anagrelide	PDE3	36 nM	*In silico* docking suggests FABPs, PARP1, HDHD3, PAR1, TTPA	0.5-11.7 μM (Platelets)		79,80
PFK	AZ PFKFB3 67	PFKFB3	11 nM	*No significant off-target inhibition of 267 screened kinases*	0.01-1 μM (Cells)		81-83

a. IC50 values for *in vitro* inhibition are from referenced sources or manufacturer data (i.e., Tocris, Selleck)

b. "Other targets" or potential "off-target" effects from references, or as noted for other kinases with <25% activity in presence of inhibitor *in vitro* (from MRC Kinase Profiling Inhibitor Database http://www.kinase-screen.mrc.ac.uk/kinase-inhibitors

c. Established working concentrations from prior studies, as referenced. Working concentrations may vary greatly from "pure" *in vitro* IC50s to account for cell permeability as well as stoichiometries with other intracellular molecules competing for target interactions (i.e., mM intracellular ATP concentrations)[84]

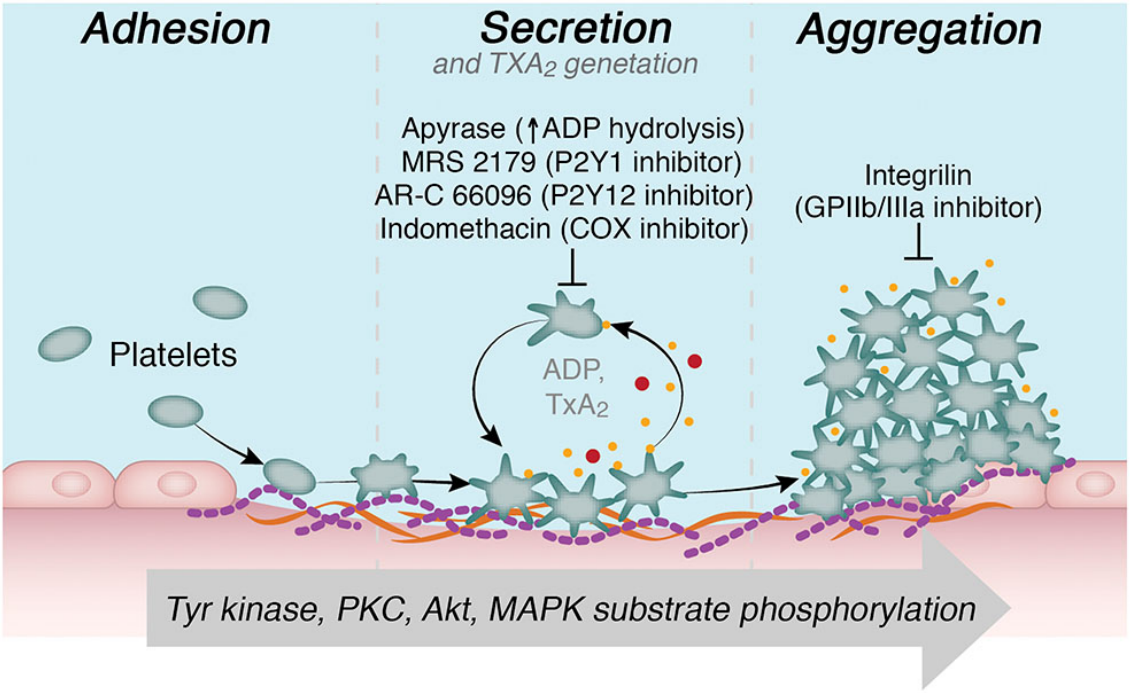

Figure S1. ***Related to Figure 1.*** **Model of platelet activation programs driven by glycoprotein receptor GPVI.** Quiescent platelets circulate in a discoid, resting state. Upon encountering signals of endothelial dysfunction or intravascular bleeding (i.e., VWF on endothelial cell surface, disorganized matrix proteins, other activating platelets, etc.), platelets tether to dysfunctional endothelium, where platelets may encounter collagen or other GPVI ligands associated with endothelial damage or inflammation. Following platelet GPVI interactions with ligands such as collagen, immunoreceptor tyrosine activation motif, or, "ITAM" signaling through FcRγ (in complex with GPVI) near-instantaneously drives platelet activation through tyrosine kinase, phospholipase and protein kinase C (PKC) signaling. At a functional level, following GPVI activation, platelets immediately mobilize dense core granules to secrete ADP, which acts as an autocrine and paracrine feedback activator of subsequent phases of platelet activation through G protein-coupled (GPCR) purinergic receptor activation (P2Y1/P2Y12). ADP secretion also serves to call additional platelets to areas of vessel injury. Depending on stimulus size and duration, activating platelets may also generate thromboxanes (i.e., TxA_2) through eicosanoid metabolism, which additionally amplify platelet activation through other GPCRs such as the prostanoid or thromboxane receptor (TP). As platelets respond to collagen, ADP, TxA_2 and other factors within the dysfunctional endothelium microenvironment, intracellular signals ultimately promote the platelet integrin $\alpha_{IIb}\beta_3$ (GPIIb/IIIa, CD41/CD61) to adopt an extracellular open/active conformation ("inside-out" activation) to mediate platelet-platelet contacts and aggregate to form hemostatic plugs in the process of vessel repair. These sequential stages of GPVI-mediated platelet activation are readily blocked by inhibition of purinergic receptor signaling (i.e., MRS 2179, AR-C 66096) or extracellular ADP depletion by apyrase. Cyclooxygenase (COX) inhibitors such as indomethacin prevent thromboxane synthesis and also limit the full progression of GPVI-mediated platelet activation. As platelet aggregation is ultimately mediated by platelet-platelet contacts through integrin $\alpha_{IIb}\beta_3$, integrin blocking agents such as Integrilin (eptifibatide) specifically prevent platelet aggregation, even when platelets are in an activated state. Each of these GPVI-driven platelet adhesion/activation, secretion, integrin activation and aggregation steps above are associated with specific intracellular signaling events mediated by a combination of tyrosine kinases, protein kinase C (PKC), Akt, MAPKs and other kinases. In this study, platelets are stimulated with the GPVI-specific agonist crosslinked collagen-related peptide (CRP-XL) in the presence and/or absence of inhibitors of feedback activation (and combinations thereof), and collected at "adhesion/activation" (Condition #1) as well as "progression" (Condition #2) phases of GPVI programs for quantitative phosphoproteomics and other analyses. See main text and Supplemental References for additional details.[85-91]

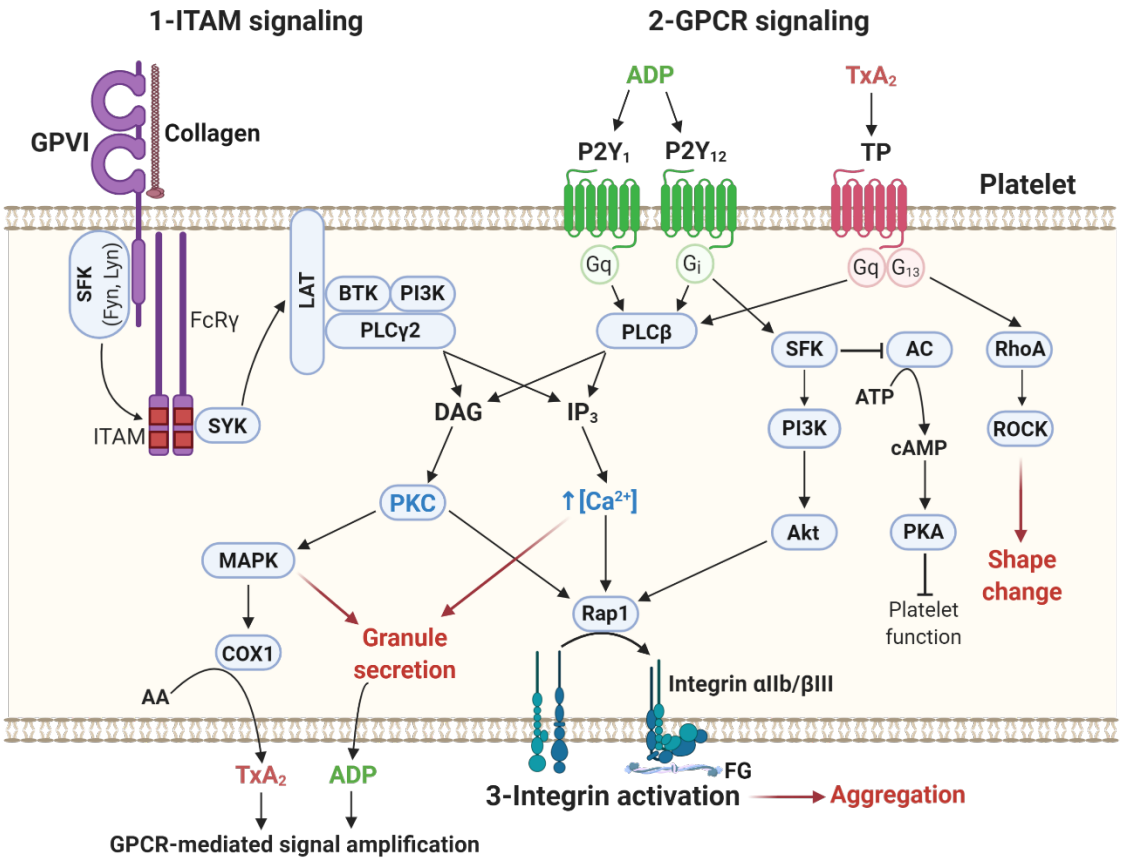

Figure S2. Overview of GPVI/ITAM and GPCR-mediated platelet activation pathways. Platelet GPVI interaction with collagen promotes the activation of Src family kinases (SFK), which are bound to the proline rich region of the GPVI cytosolic tail. SFK subsequently phosphorylates the immunoreceptor tyrosine-based activation motif (ITAM) of FcRγ, which promotes signaling via SYK and LAT-mediated activation of phospholipase C gamma 2 (PLCγ2) that releases the lipid mediators diacylglycerol (DAG) and inositol-3-phosphate (IP_3). DAG activates Protein kinase C (PKC) pathways leading to Mitogen activated protein kinases (MAPK) activation and subsequent conversion of arachidonic acid (AA) into thromboxane A2 (TxA_2) by cyclooxygenase 1 (COX1). IP_3 promotes calcium release from the endoplasmic reticulum promoting an increase in cytosolic Ca^{2+} concentration, which induces granule secretion, including adenosine diphosphate (ADP) release from dense granules, and integrin $\alpha_{IIb}\beta_3$ activation. The activated form of integrin $\alpha_{IIb}\beta_3$ mediates platelet aggregation upon binding to soluble adhesive proteins including fibrinogen (FG). ADP and TxA_2 mediate an autocrine and paracrine feedback activating loop via G protein-coupled receptors (GPCR). GPCR signaling downstream of ADP and TxA_2 involves the activation of PLCβ, which mediates a second wave of signaling via PKC activation and increased Ca^{+2} concentration. Purinergic signaling via $P2Y_{12}$ also involves the blockade of platelet inhibitory pathways such as adenylate cyclase (AC) and protein kinase A (PKA). TxA_2 signaling via TXA_2 receptor (TP) is also involved in cytoskeletal changes via RhoA and Rho-associated protein kinase (ROCK). See main text and Supplemental References for additional details.[85-91]

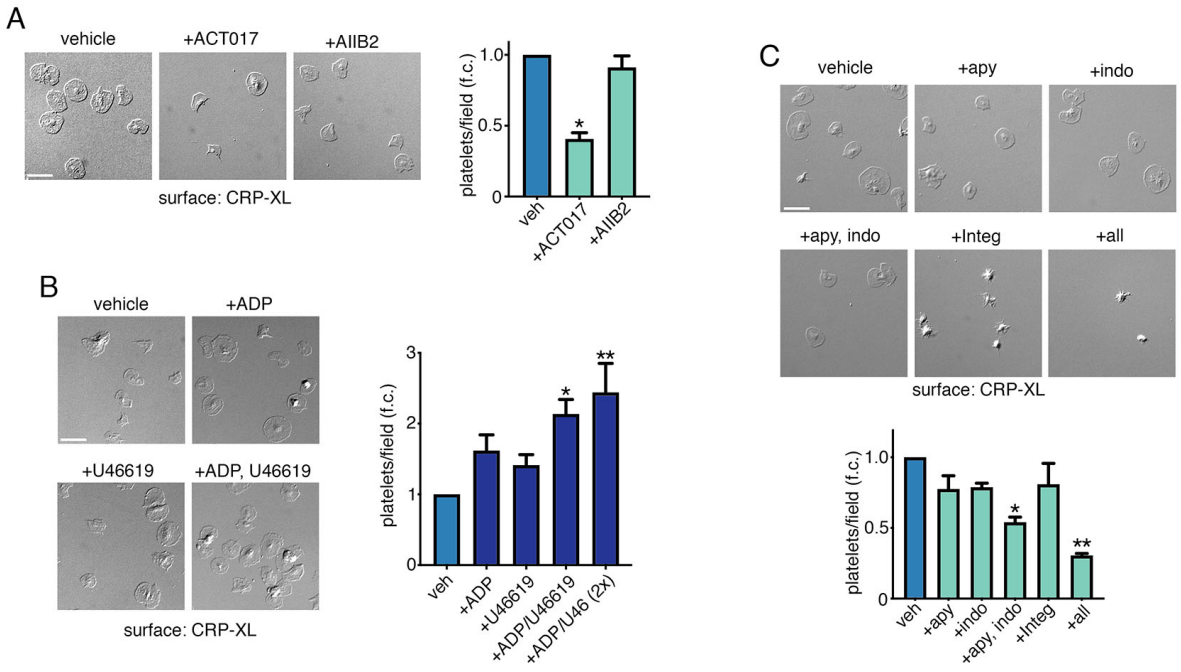

Figure S3. ***Related to Figure 1.*** **Platelets adhere to CRP-XL coated cover glass in a GPVI-dependent manner that is enhanced by ADP, thromboxane and integrin activation. (A)** Replicate samples (n=3) of washed human platelets (2×10^7/ml) were incubated on cover glass coated with 2 μg/ml CRP-XL (and subsequently blocked with 2% denatured BSA) in the presence of the GPVI blocking Fab ACT017 (50 μg/ml), the integrin $\alpha_2\beta_1$antibody AIIB2 (50 μg/ml) or vehicle alone. Scale bar = 10 um. Platelets per field were counted. *p<0.0001 **(B)** Replicate samples (n=3) of washed human platelets (2×10^7/ml) were incubated with CRP-XL-coated cover glass in the presence of ADP (20 μM) , thromboxane analog (U46619, 10 μM), a combination of ADP+U46619 at 1x and 2x concentrations. *p=0.01; **p=0.002 **(C)** Replicate samples (n=3) of washed human platelets (2×10^7/ml) were incubated with CRP-XL-coated cover glass in the presence of apyrase, indomethacin, Integrilin, or a combination of all 3 reagents (+all). Platelets per field were quantified. *p=0.004; **p=0.0001

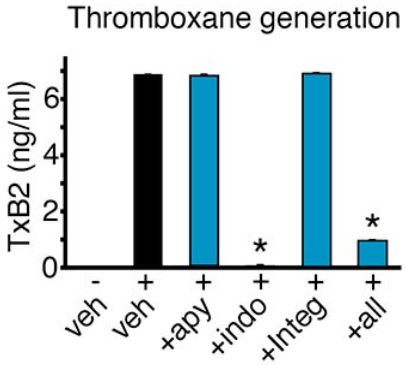

Figure S4. ***Related to Figure 1.*** **Indomethacin inhibits platelet thromboxane generation in response to CRP-XL.** Replicate samples (n=3) of washed human platelets (2×10^8/ml) were incubated with apyrase (2 U/ml), indomethacin (10 μM), Integrilin (20 μg/ml) and a combination thereof ("+all") or vehicle alone ("veh"). Following the addition of CRP-XL (10 μg/ml, 5 min, indicated with "+"), samples were centrifuged and supernatants were analyzed for thromboxane TxB_2 (stable metabolite of TxA_2) content by ELISA (Enzo Life Sciences) (*p<0.0001).

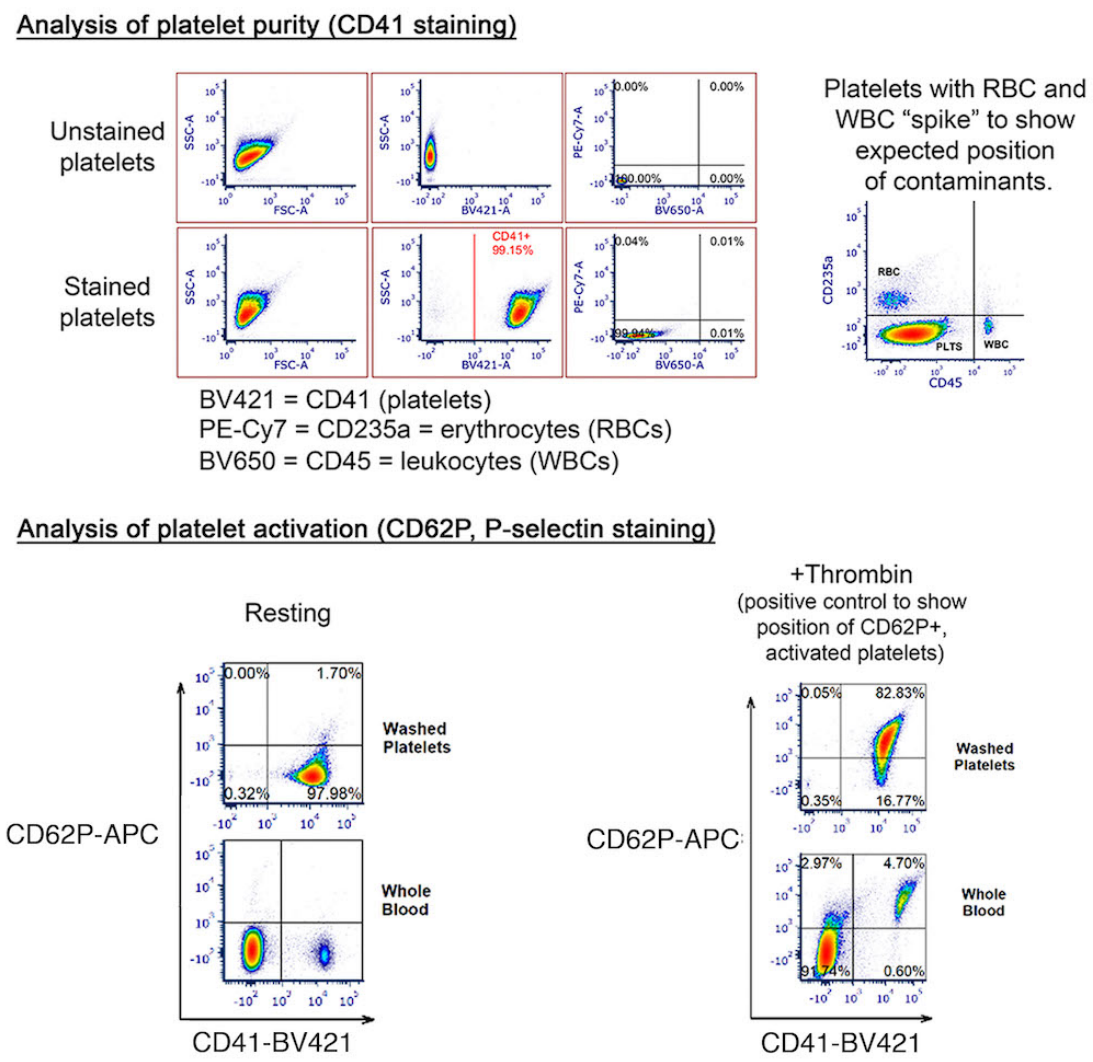

Figure S5. ***Related to Figures 2-3.*** **Platelet sample purity as determined by flow cytometry analysis.** A representative set of flow cytometry assay results for the platelet preparations in this study are shown. *Upper*: This specific human washed platelet preparation was found to contain 99.15% CD41-positive cells (platelets) and 0.01% CD235a-positive cells (RBCs) and 0.01% CD45-positive cells (WBCs). On the upper right, a platelet preparation spiked with RBCs and WBCs prior to staining is shown to demonstrate the expected positions of contaminating cells. *Lower*: Purified platelets (and platelets in whole blood prior to purification) are not activated and in a quiescent, resting state (1.70% "P-selectin" CD62P-positive cells). Platelets stimulated with thrombin (1 U/ml, 5 min) serve as a positive control to show the expected position of activated platelets and to demonstrate that platelets are functionally responsive.

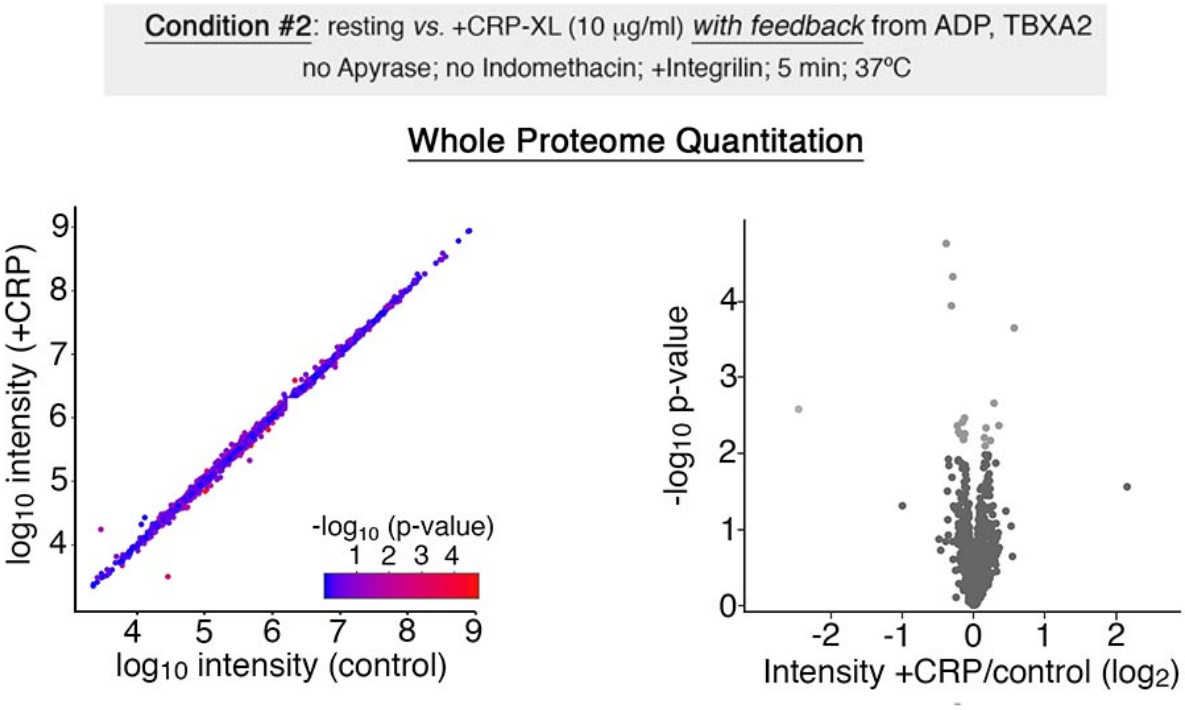

Figure S6. ***Related to Figures 2-3.*** **Whole proteome, multiplex quantitation of resting vs. +CRP-XL activated platelet samples.** Aliquots of matched "resting" (n=5) and "activated" (n=5) platelet lysates from Condition #2 studies were digested, purified, and TMT-labeled for 10-plex quantitative analysis of total protein levels. As seen above, stimulation of platelets with CRP-XL (5 min, 37°C) is associated with negligible changes in total protein levels. We find that of 3,234 quantified proteins, 18, 9 and 0 proteins are noted as potential differential expression candidates at low (FDR<0.1), medium (FDR<0.05) and high (FDR<0.01) stringency thresholds, respectively. See Results, Table S1 and Supplemental materials for additional details.

This data is available in interactive form through the START App at https://kcvi.shinyapps.io/STARTapp_515_total/

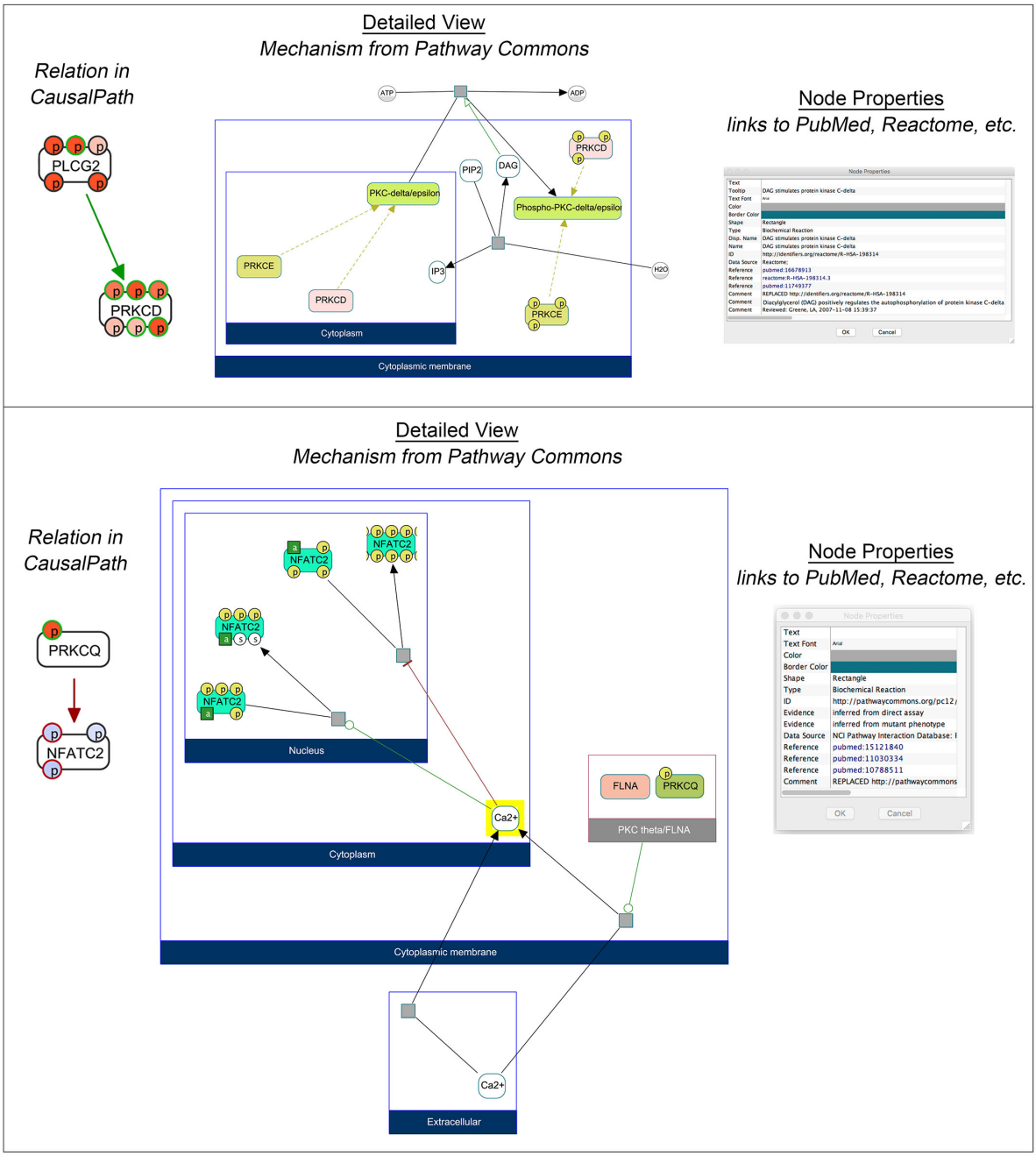

Figure S7. ***Related to Figure 4.*** **Examples of relations modeled by CausalPath.** In addition to direct kinase substrate relations, CausalPath models more complex relations between phosphorylated proteins. *Upper*. Example of "phosphorylation of PLCG2 (PLCγ2) causes phosphorylation of PRKCD (PKCδ)". Here, phosphorylation of the phospholipase PLCG2 activates PLCG2; activated PLCG2 produces diacylglycerol (DAG) and inositol trisphosphate (IP3) from phosphatidylinositol 4,5-bisphosphate (PIP2); DAG activates PRKCD; finally, active PRKCD autophosphorylates PRKCD. CausalPath represents this relation as a single green arrow between PLCG2 and PRKCD. Clicking on this green arrow in ChiBE software brings up a "Detailed view" of this relationship. Nodes (gray boxes) link to references, including PMID: 16678913, PMID: 11749377 and Reactome pathway: R-HSA-198314 ("DAG stimulates protein kinase C-delta"; https://reactome.org/content/detail/R-HSA-198314). *Lower*. Example of less intuitive relation "PRKCQ dephosphorylates NFATC2". The Detailed view of this relation notes that following phosphorylation (and activation) of PRKCQ (PKCθ), increases an intracellular calcium flux; then, activation of the (calcium-dependent) phosphatase calcineurin (PP2B) dephosphorylates NFATC2 (NFAT1 protein). This set of detailed relations is represented by a single red arrow, summarizing that phosphorylation of PRKCQ is causally associated with dephosphorylation of NFATC2 through a series of events, referenced by PMID: 10788511, PMID: 11030334 and PMID: 15121840

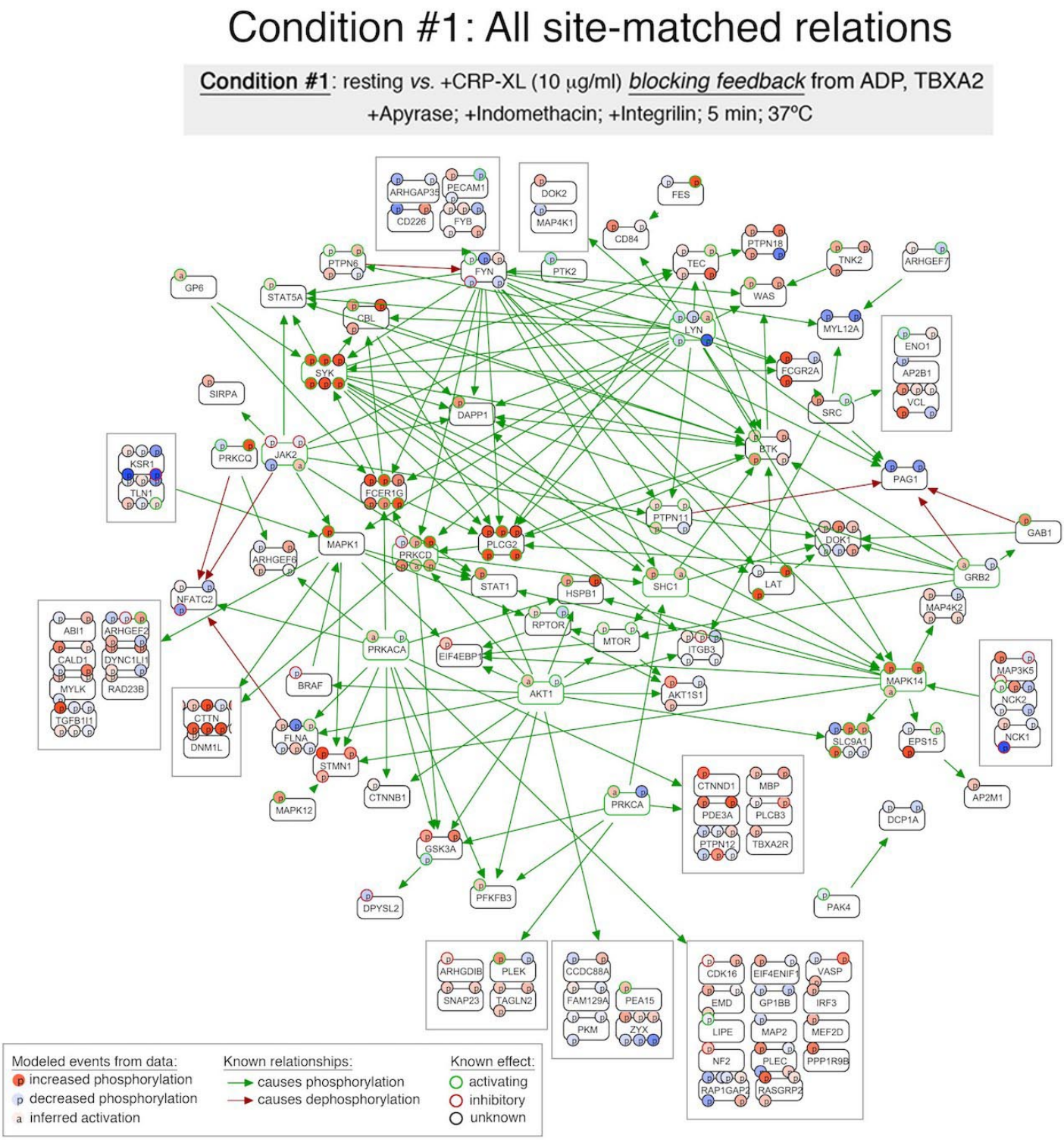

Figure S8. ***Related to Figure 4.*** **Site-matched causal relations for Condition #1.** CausalPath mapped 229 high-confidence, site-specific signaling relations amongst 205 phosphorylation sites on 118 proteins from 982 increasing and 1,184 decreasing phosphorylation events measured in Condition #1 experiments (feedback activation from ADP, TxA_2 inhibited). See Results and Figure 4 for complete Legend details.

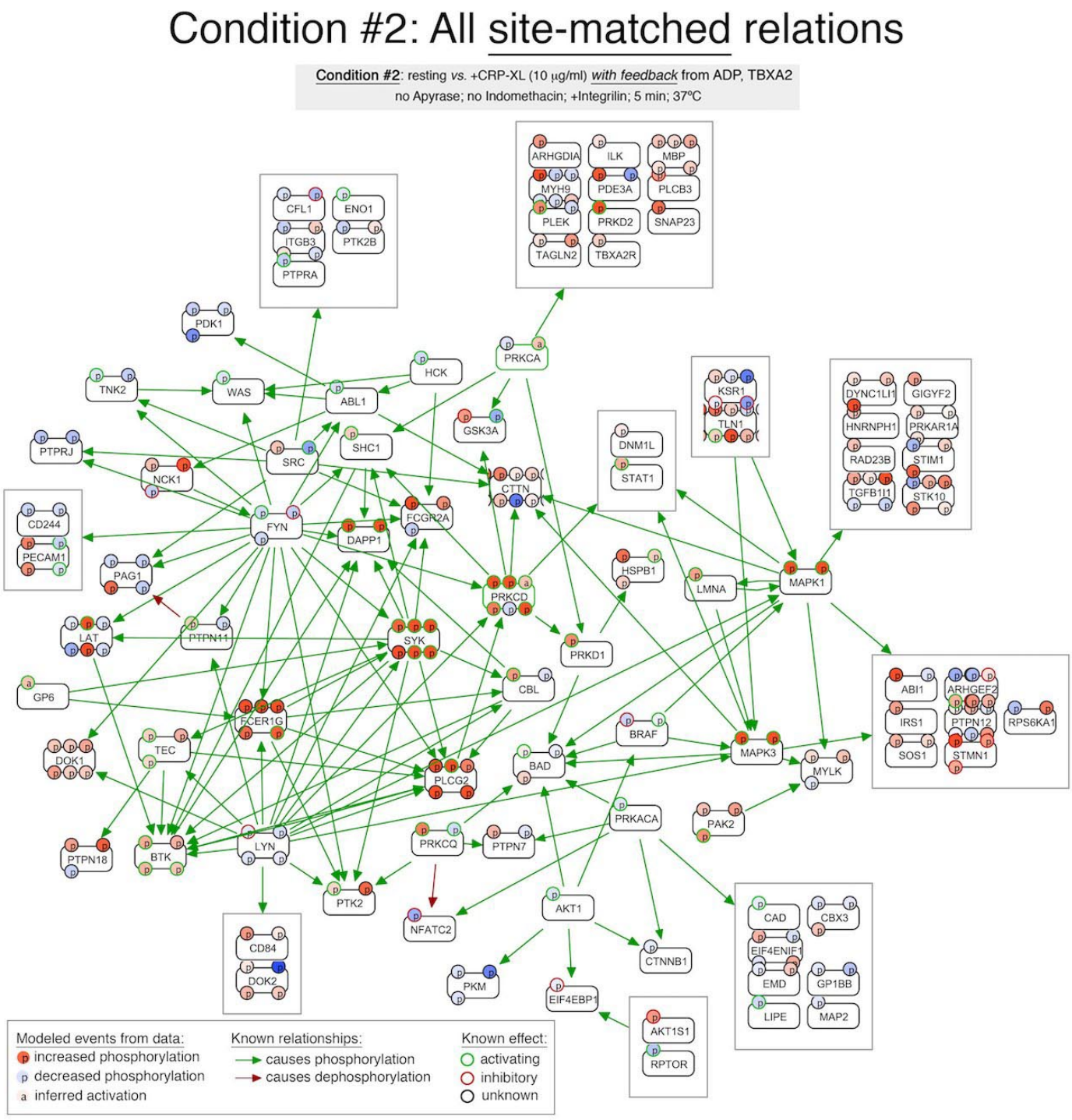

Figure S9. ***Related to Figure 4.*** **Site-matched causal relations for Condition #2.** CausalPath mapped 196 high-confidence, site-specific signaling relations amongst 171 phosphorylation sites on 102 proteins from 1,294 increasing and 1,305 decreasing phosphorylation events measured in Condition #2 experiments (feedback from ADP, TxA_2 permitted). See Results and Figure 4 for complete Legend details.

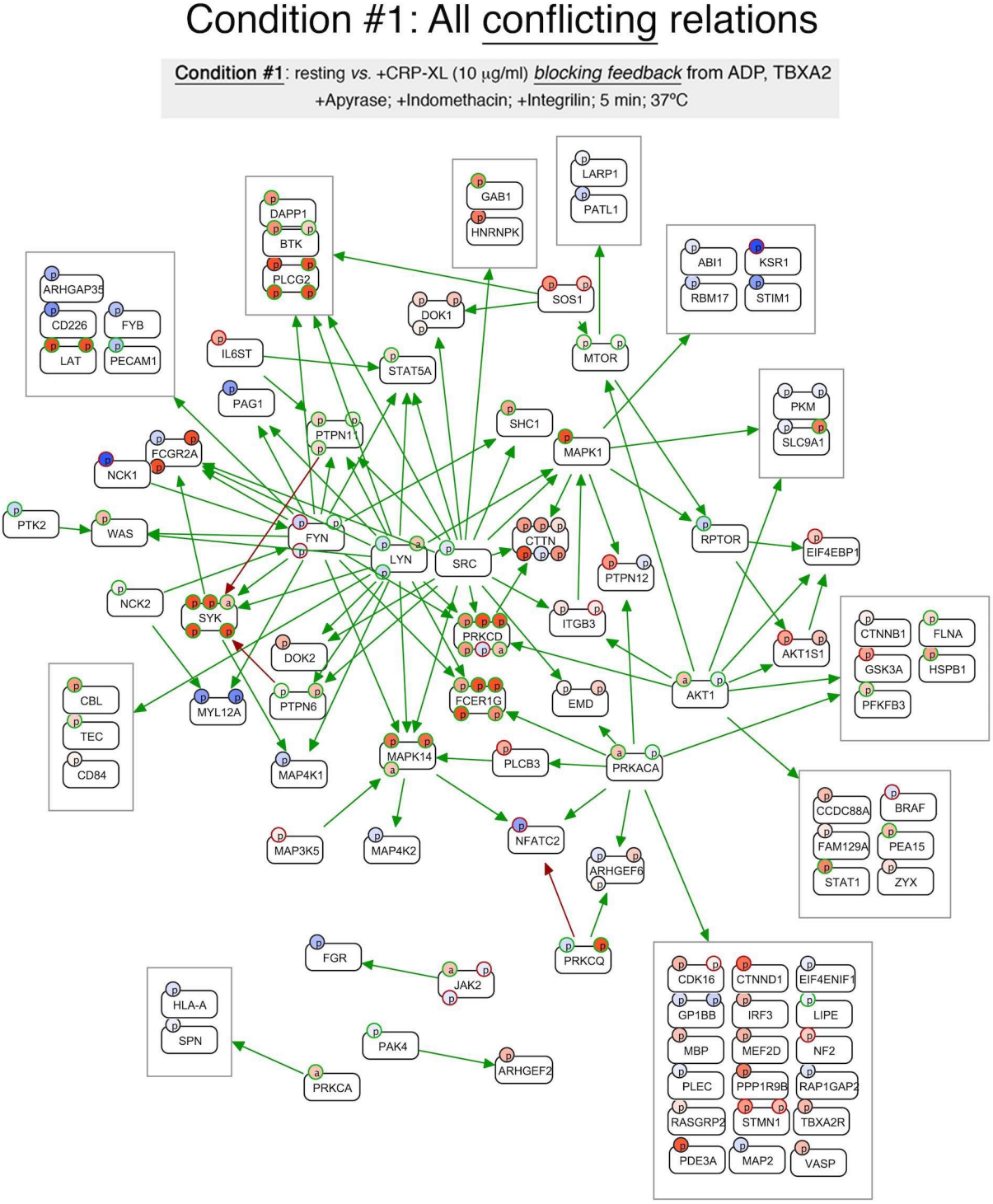

Figure S10. ***Related to Figure 4.*** **Conflicting pathway relations for Condition #1.** CausalPath noted 145 conflicting relations between 97 proteins for Condition #1 data. Here, kinase activation and substrate phosphorylation patterns do not match. For instance, ERK2 (MAPK1) is found to be activated in phosphoproteomics data, and several ERK2 substrate sites are found to increase in phosphoproteomics data (i.e., ABI1 S_{225}, ARHGEF2 S_{679}); however, several ERK2 substrate sites are also found to be significantly dephosphorylated in phosphoproteomics data (i.e., ABI1 S_{183}, STIM1 S_{575}). We suspect that many such dephosphorylations are likely due to regulatory events that rapidly occur in GPVI signaling and may represent important targets of regulation in platelet activation programs for future study.

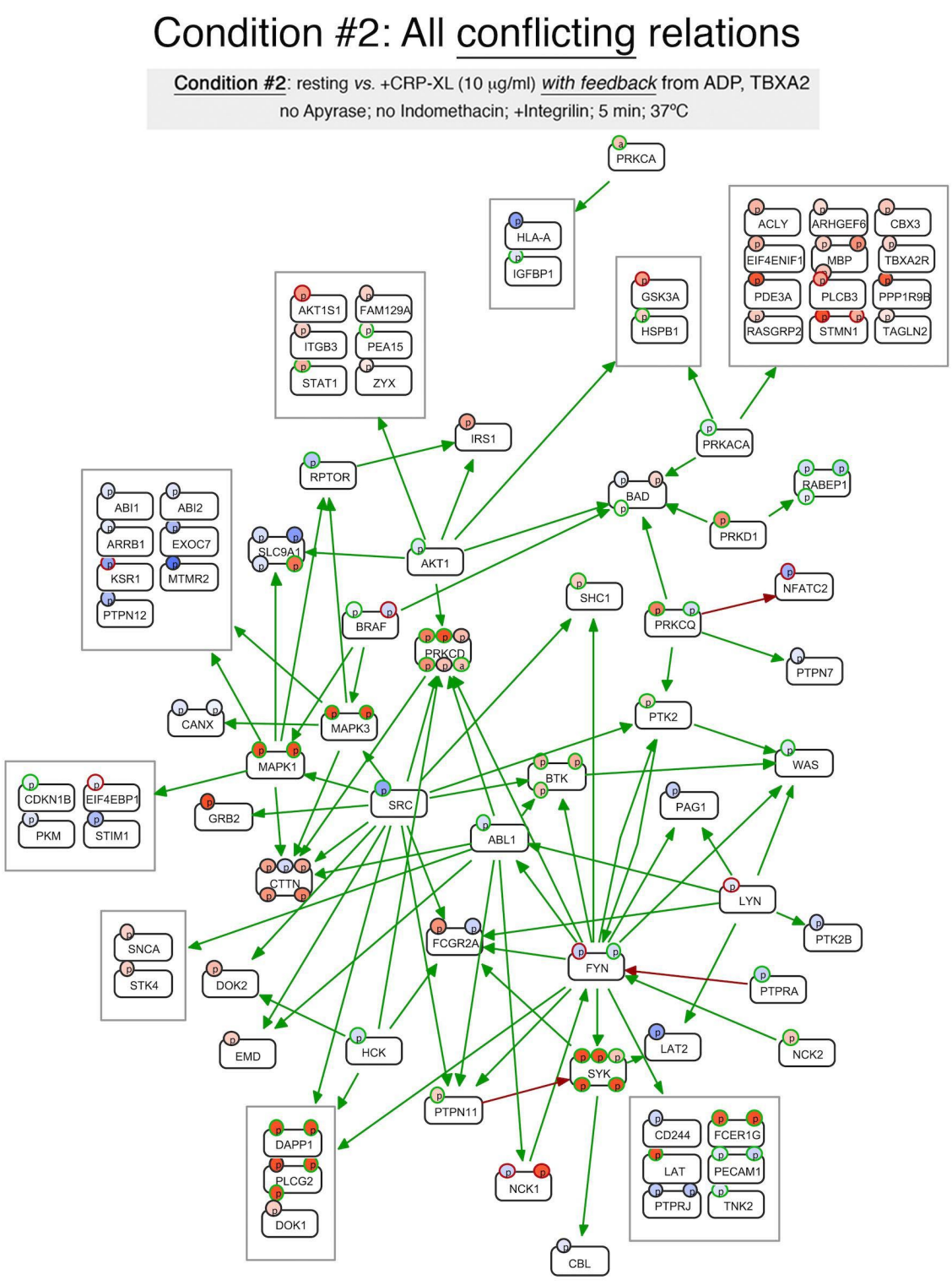

Figure S11. ***Related to Figure 4.*** **Conflicting pathway relations for Condition #2.** CausalPath noted 128 conflicting relations for 84 proteins for Condition #2 data, where kinase activation and substrate phosphorylation patterns do not match. See Figure S8 and Results for further details.

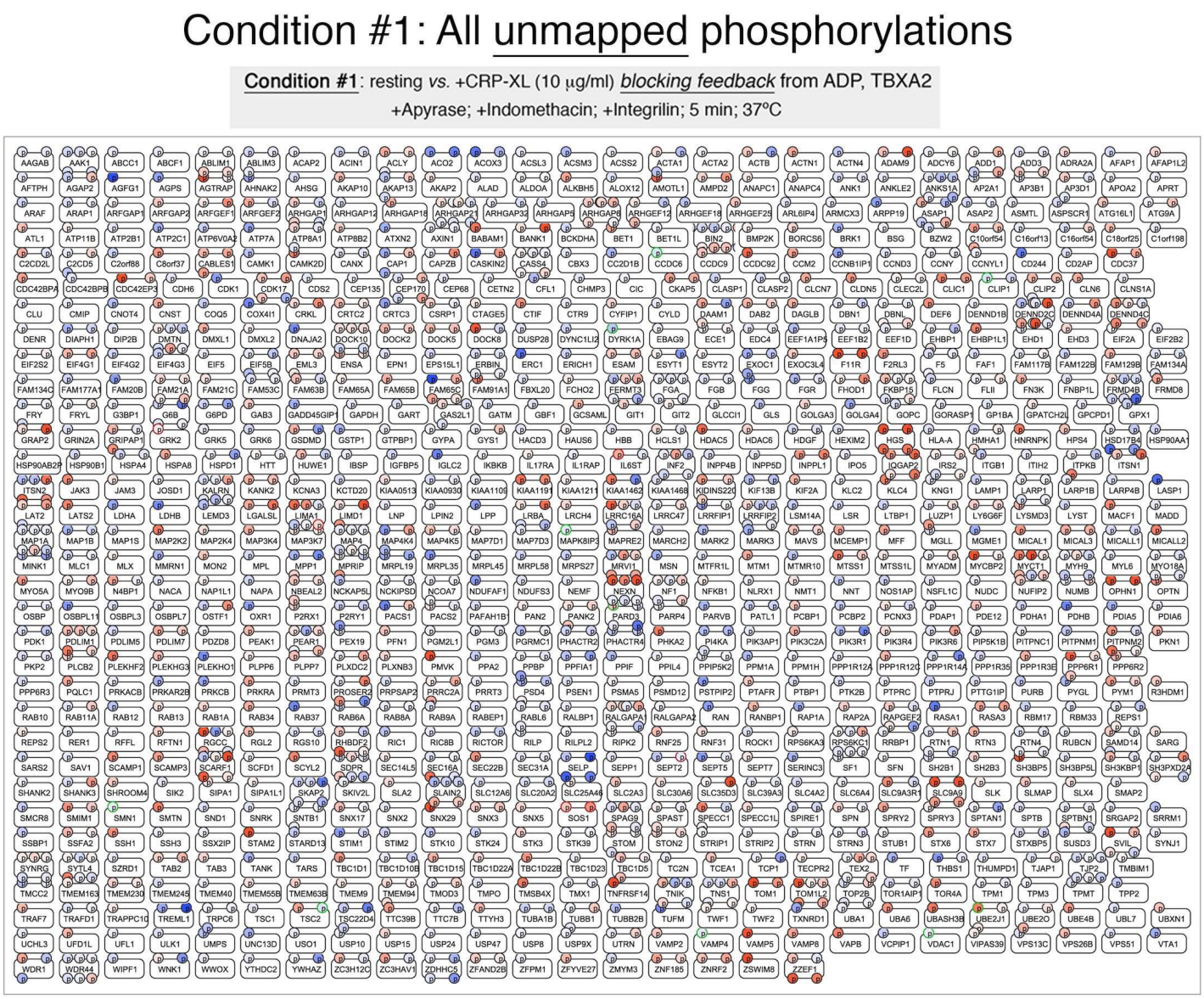

Figure S12. ***Related to Figure 4.*** **All unmapped dynamic phosphorylation sites for Condition #1.** A graphic representation of all significant phosphorylation site changes measured in phosphoproteomics data for Condition #1 that did not match any causal priors from Pathway Commons or place into causal models generated for Condition #1.

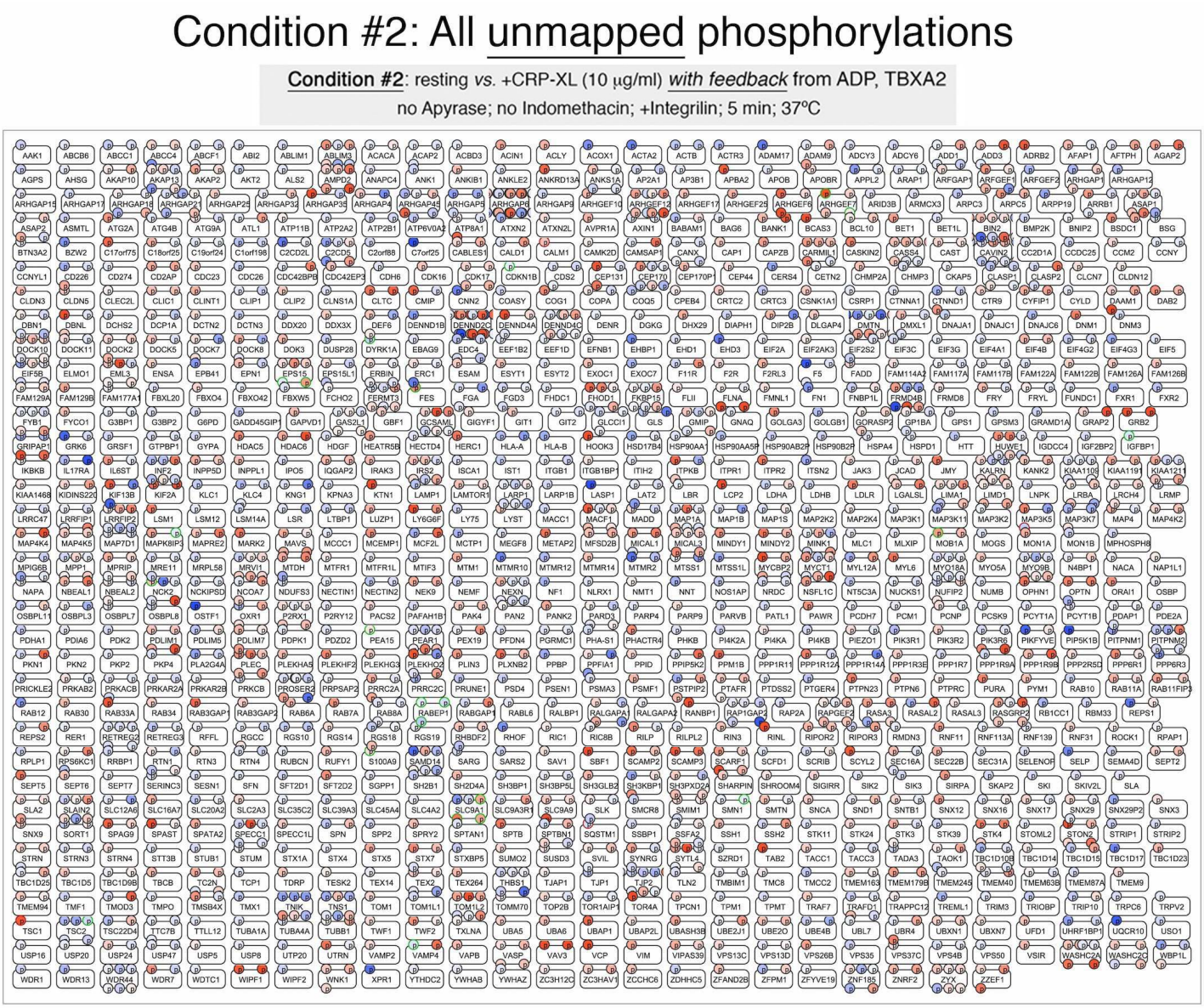

Figure S13. ***Related to Figure 4.*** **All unmapped dynamic phosphorylation sites for Condition #2.** A graphic representation of all significant phosphorylation site changes measured in phosphoproteomics data for Condition #2 that did not match any causal priors from Pathway Commons or place into causal models generated for Condition #2.

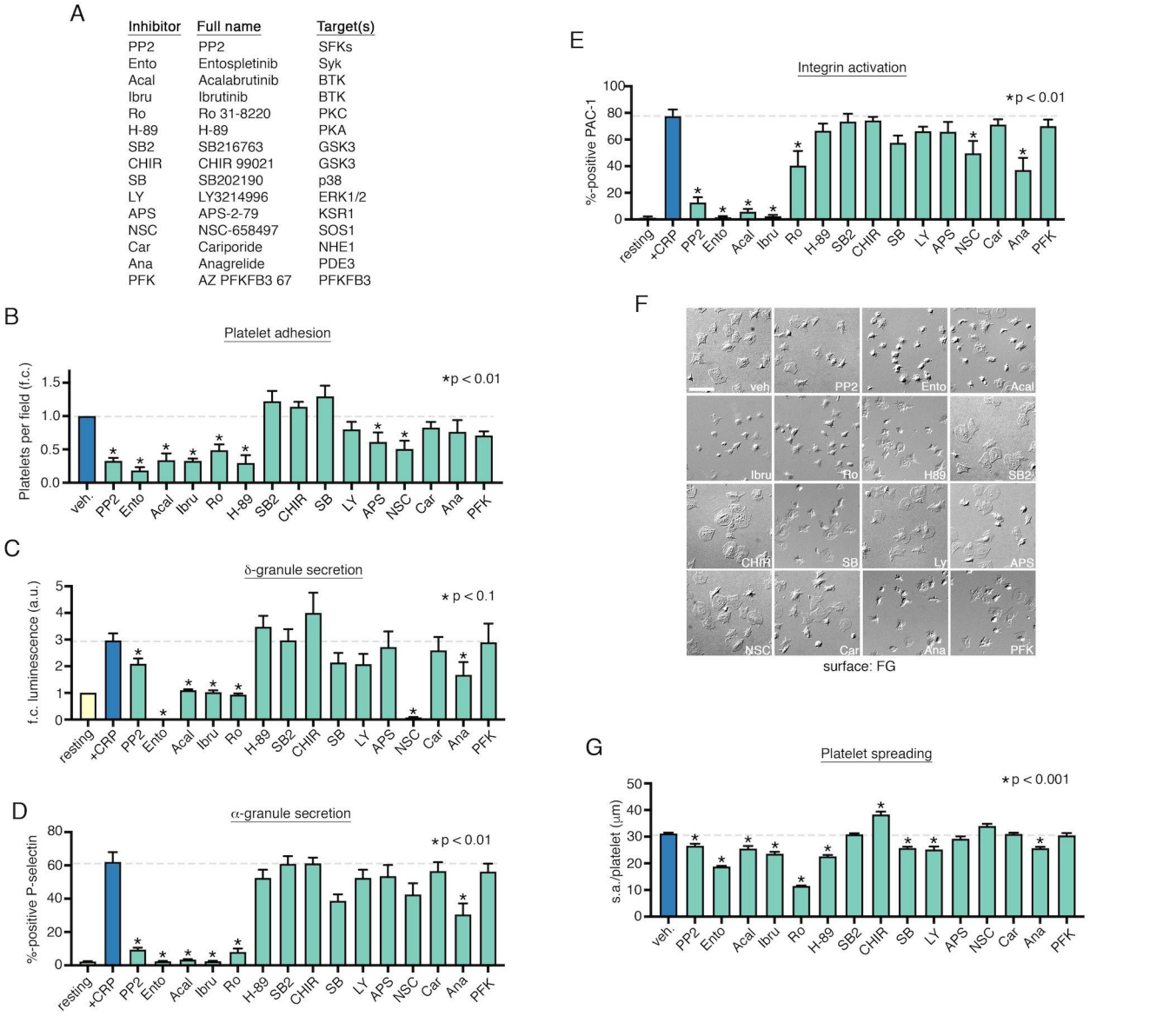

Figure S14. ***Related to Figure 5.*** **Effects of selected inhibitors on GPVI-mediated platelet adhesion, secretion and integrin activation.** Following pretreatment with pharmacological inhibitors against targets of interest listed in **(A)** and Supplemental Table S3, **(B)** replicate samples (n=3) of washed human platelets (2×10^7/ml) were incubated with CRP-coated cover glass. After 30 min, cover glass were washed, platelets were fixed and visualized by DIC microscopy. Platelets per field were quantified for 3 visual fields per condition to determine fold-change (f.c.) differences in number of adherent platelets relative to vehicle treatment alone ("veh.", 0.1% DMSO). **(C)** Platelets were preincubated with inhibitors, as indicated, prior to addition of Chrono-lume reagent and CRP-XL to measure ATP-dependent luciferase activity as an indicator of platelet ADP release and δ-granule secretion. Fold-change (f.c.) increases in luciferase activity relative to resting control are shown (n>4). **(D)** Platelets were pretreated with inhibitors, as above, prior to stimulation with 10 μg/ml CRP-XL in the presence of anti-CD62P-APC. After 30 min, samples were analyzed by flow cytometry. The percentage of CD62P positive platelet-gated events per condition quantifies platelet α-granule secretion. **(E)** Parallel flow cytometry studies of platelets incubated with FITC-PAC-1 quantify integrin $\alpha_{IIb}\beta_3$ activation. After 30 min, samples were analyzed by flow cytometry to determine the percentage of FITC-PAC-1 positive, platelet-gated events per condition, as shown. **(F)** Replicate samples (n=3) of washed platelets were pretreated with inhibitors, as indicated, prior to incubation on cover glass coated with human fibrinogen (a ligand of the platelet integrin $\alpha_{IIb}\beta_3$). The ability of platelets to adhere to and spread upon fibrinogen surfaces serves as an indicator of ITAM-related signaling events following integrin activation.[3,85] After 45 min, cover glass were washed, fixed and imaged by DIC microscopy. Individual platelet surface areas (s.a., μm^2/platelet) were determined for 200 platelets per condition per experimental replicate using Image J, as quantified in **(G)**. These results are summarized together in Figure 5C.

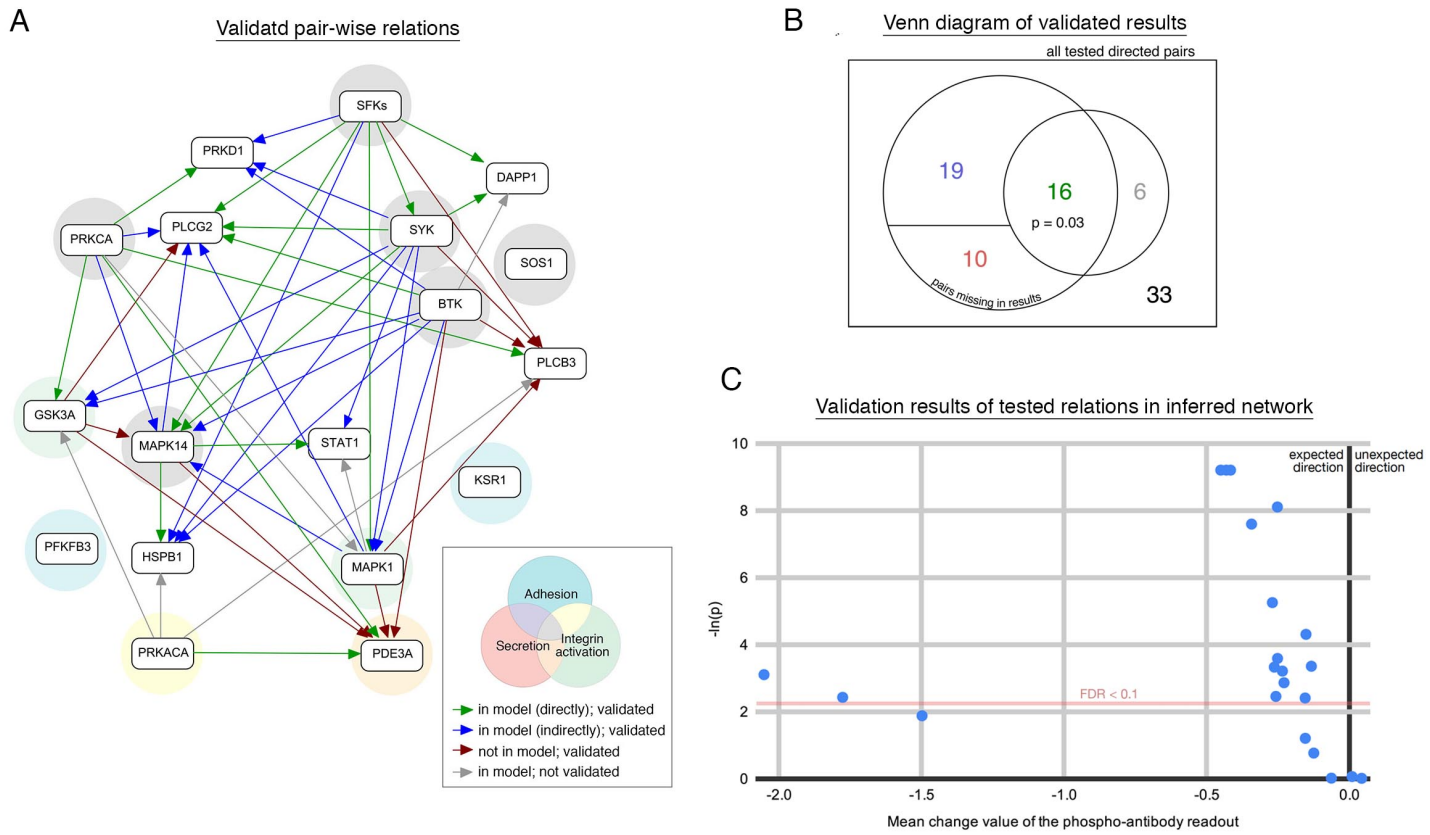

Figure S15. ***Related to Figure 5.*** **Analysis of all validated platelet signaling and function relations in CausalPath model. (A)** From all combinations of inhibitor-antibody pairs in Figure 5A-B (84 pairs, excluding the cases where inhibited and measured proteins are the same), 45 pairs were valid (0.1 FDR), including 16 of 22 inferred relations. Arrows represent modeled and validated GPVI signaling relations between proteins, as indicated by color. Shaded circles indicate supporting experimental evidence for specific pathway nodes in GPVI-mediated platelet adhesion (blue), secretion (red) and integrin activation (green), and combinations thereof, colored according to function (gray=associated with all functions tested). **(B)** Validation classes are shown on a Venn diagram. Valid and inferred pairs were significantly overlapping ($p = 0.03$, Fisher's exact test); 19 of the other validated pairs can be explained by a multi-step path in the inferred model. **(C)** The mean change values versus their significance of the validations of the tested relations in the result network. The dots in this plot correspond to the green and gray relations in (A). Gray relations map to the 6 dots below the threshold line. 20 of the 22 relations are changed in the negative direction as expected. All significant changes are toward the expected direction.

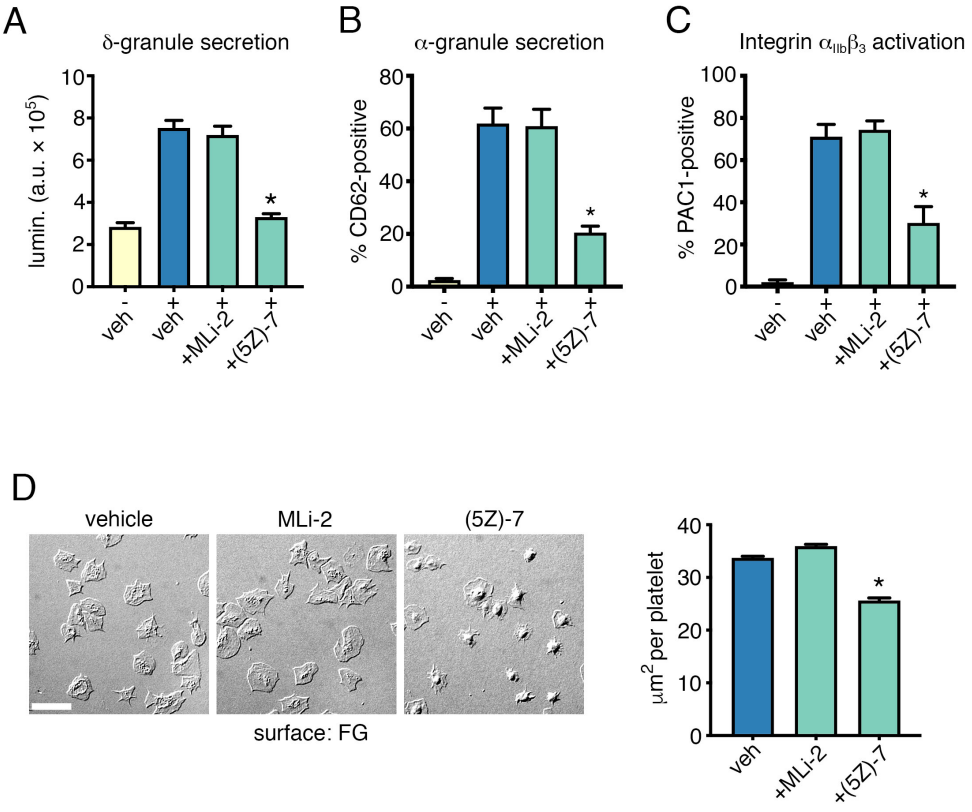

Figure S16. ***Related to Figure 6.*** **Effects of Rab7A S72 phosphorylation inhibitors on platelet function.** (A) Washed human platelets were prepared as in Figure 1 and preincubated with vehicle (0.1% DMSO), LRRK2 inhibitor MLi-2 (1μM), or TAK1 inhibitor (5Z)-7-Oxozeaenol (10 μM) "(5Z)-7") for 10 min prior to stimulation with CRP-XL (10 μg/ml) and analysis for **(A)** δ-granule secretion, **(B)** α-granule secretion and **(C)** integrin activation as detailed in Figures 1 and S14. **(D)** Aliquots of vehicle and inhibitor treated platelets were also analyzed for spreading on fibrinogen using methods detailed in Figure S14. *P<0.01